

# SKBF TECHNICAL KBS REPORT

**83-25**

## Feasibility study of electron beam welding of spent nuclear fuel canisters

A Sanderson  
T F Szluha  
J L Turner  
R H Leggat

The Welding Institute Cambridge,  
The United Kingdom April 1983

**SVENSK KÄRNBRÄNSLEFÖRSÖRJNING AB / AVDELNING KBS**

Swedish Nuclear Fuel Supply Co/Division KBS

MAILING ADDRESS: SKBF/KBS, Box 5864, S-102 48 Stockholm, Sweden

Telephone 08-67 95 40

FEASIBILITY STUDY OF ELECTRON BEAM WELDING  
OF SPENT NUCLEAR FUEL CANISTERS

A Sanderson  
T F Szluha  
J L Turner  
R H Leggatt

The Welding Institute  
Cambridge, The United Kingdom April 1983

This report concerns a study which was conducted for SKBF/KBS. The conclusions and viewpoints presented in the report are those of the author(s) and do not necessarily coincide with those of the client.

A list of other reports published in this series during 1983 is attached at the end of this report. Information on KBS technical reports from 1977-1978 (TR 121), 1979 (TR 79-28), 1980 (TR 80-26), 1981 (TR 81-17) and 1982 (TR 82-28) is available through SKBF/KBS.

FEASIBILITY STUDY OF ELECTRON BEAM WELDING  
OF SPENT NUCLEAR FUEL CANISTERS

The Welding Institute  
Abington Hall, Abington Cambridge, The United Kingdom  
April 1983

1. Feasibility Study of EB Welding of Spent  
Nuclear Fuel Canisters - Phase I

A Sanderson

2. Feasibility Study of Electron Beam Welding  
of Spent Nuclear Fuel Canisters -  
Phases II and III

A Sanderson, T F Szluha and J L Turner

3. Appendix: Residual Stress Measurements in  
an EB Welded Copper Disc

R H Leggatt

## SUMMARY

A thick walled copper container is presently the prime Swedish alternative for encapsulation of spent nuclear fuel. In order to demonstrate the feasibility of encapsulating high-level nuclear waste in copper containers, a study of electron beam welding of thick copper has been performed. Two copper qualities have been investigated, oxygen free high conductivity (OFHC) copper and phosphorous desoxydized high conductivity copper (PDO). The findings in this study are summarized below.

In 100 mm thick copper penetration can be achieved at power level of about 75 kW (typically 150 kV x 500 mA) at welding speed of 100 mm/min. The welds in OFHC copper made under these conditions are free from major defects during constant welding conditions. The welds in PDO copper show a microporosity level considerably higher than those in OFHC copper, but no major defects are produced in the welds in PDO copper.

In the ending of the weld (ie the fade out) it is still not possible to completely eliminate root and cold-shut defects.

A semi-full-scale lid weld has been performed successfully.

Automatic ultrasonic C-scan has been shown to be useful in detecting and displaying defects, but some problems still remain with defect sizing. The different specimens of OFHS copper had different attenuation of the ultrasonic signal, forged copper showing a far lower attenuation than hot extruded copper, indicating that attention must be paid in choosing copper that allows accurate ultrasonic testing.

Residual stresses in the welded zone has been measured and are found to lie in the range  $-32\text{N/mm}^2$  to  $+36\text{N/mm}^2$ . The peak stress was less than half the assumed value of the proof stress of the fused metal.

# THE WELDING INSTITUTE

PLEASE REPLY TO RESEARCH LABORATORY ABINGTON HALL ABINGTON CAMBRIDGE CB1 6AL  
Telephone CAMBRIDGE 0223 891162 Telegrams WELDASERCH CAMBRIDGE Telex 81183 Telefax (0223) 892588

LONDON OFFICE 54 PRINCES GATE EXHIBITION ROAD LONDON SW7 2PG  
Telephone 01-584 8556 Telegrams WELDINST LONDON SW7

Our Ref: AS/BCT/547.82

1st September, 1982

## FEASIBILITY STUDY OF EB WELDING OF SPENT NUCLEAR FUEL CANISTERS - PHASE I

The following letter report summarises the work carried out to date on this project.

### 1. EQUIPMENT

The majority of the welding was carried out on the Welding Institute 75kW EB1 (2m x 2m x 2m) machine which is equipped with a magnetic trap device. A working distance of 150mm was employed and all welding was performed in the HV mode at a vacuum pressure of approximately  $5 \times 10^{-3}$  torr.

### 2. MATERIALS

Most of the welds were made in the OFHC copper supplied from Outokumpu Oy to BS 3839 : 1965 and ASTM F68-77. Welds were later made in phosphorus deoxidised material for comparison, this was supplied by Granges Metallverken.

The OFHC copper was received as bar stock in 106 x 56mm<sup>2</sup> and 106 x 106mm<sup>2</sup> sections whereas the PDO material was supplied only as 100 x 50mm bar.

### 3. EXPERIMENTAL APPROACH

In order to determine the likely beam power requirements, melt runs were initially made in the 56mm thick OFHC copper at a welding speed of 250mm/min. After several parameter optimisation experiments

Continued/2

Mr. L. Werme,  
SKBF

Our Ref: AS/BCT/547.82  
1st September, 1982

---

it was established that a power level of at least 150kV x 240mA was required to just penetrate this thickness, but to produce a melted zone of any appreciable width a power of 150kV x 350mA was necessary. Some experiments were also made at this stage using transverse square-wave oscillation in an attempt to prevent undercutting on the top bead but no significant progress was made. A typical section taken of one of these melt runs indicated sound weld metal but a slightly tapered fusion zone.

Melt runs were subsequently made in the OFHC material through the 106mm thickness. Specimen size was initially 106 x 56 x 330mm. After optimising focus coil current, penetration was just achieved with a power level of 150kV x 500mA at a speed of 250mm/min. A metallographic section indicated a fairly parallel fusion zone with a mid-section width of approximately 5mm.

The body of the weld was free from significant defects but root porosity extended for some 20mm into the thickness of the material. This illustrated that in order to achieve greater penetration depth, combined with a more parallel fusion zone, whilst avoiding root defects, lower welding speeds would be necessary combined with backing material.

Some melt run trials were carried out on the Welding Institute EB2 installation which embodies a double focussing lens system enabling better control of beam profile. The results were quite promising but unfortunately traverse problems made it necessary to curtail the work.

When work was continued on the EB1 machine attempts were made to increase penetration by the use of longitudinal oscillation at a frequency of 2KHz. Oscillation amplitudes of between 2 and 7.5mm were tried. No significant increase in penetration was noted. It was therefore decided to explore the possibility of welding at lower speeds. Normally for high conductivity materials such as copper, fairly high welding speeds are usually used so that the bulk heat flow does not exceed the weld-pool motion, otherwise preheating of the material occurs which can result in thermal runaway. Under these conditions the weld width and penetration depth can gradually increase to the point where the weld-pool becomes unstable. However, for 'backed' material, where the thickness of the backing can be very large as in the case of the copper canisters, it was thought this problem might not arise. Trials were therefore carried out at welding speeds of 50mm/min and 100mm/min. Remarkably the first melt runs made on 106 x 56 x 330mm<sup>3</sup> blocks did not show any great tendency for weld-pool

Continued/3

Mr. L. Werme  
SKBF

Our Ref: AS/BCT/547.82  
1st September, 1982

---

instability, although the penetration gradually increased as the block became hot. When the test was repeated on cold material, with 56mm thick backing, the beam fully penetrated the backing after welding for 2 minutes.

### 3.1. TEST SPECIMEN W11

Since the previous results looked promising it was decided to produce proper welds in more sizeable pieces as shown in Fig. 1. The joint was lightly clamped and tack welded prior to welding at a power level of 150kV x 50mA with a weld speed of 100mm/min. The weld was subsequently completed at a speed of 100mm/min using a power level of 150kV x 500mA with a focus coil current of 1.400Amps. In this case the backing was only just penetrated at the end of the weld. The weld was sliced out of the block and radiographed perpendicular to the joint plane. The enclosed copy of the radiograph (neg. no. 50890) shows very few defects in the body of the weld (NB the small patch of indication adjacent to the identification 'A' are not defects but adhering dust particles on the original radiograph). Some small cavities have been formed at the start (B) and finish (A) of the weld but all of the root defects have been confined to the backing material. The root defects serve to indicate the gradual increase in penetration followed by a rapid increase towards the end of the weld. Top surface cavitation has been limited in this case to approximately 5mm.

Sections were taken from specimen W11, 50mm from either end of the weld and from the central region. No significant defects were found. The fusion zone was distinguishable from the parent metal by slight differences in grain size and orientation, absence of twins and faint striations running through the depths of the weld. The latter were only evident under certain etching conditions and are thought to be merely lattice discontinuities causing preferential etching. Some microporosity was evident in all of the sections but this appeared as rounded pores generally less than 0.5mm in diameter. The fusion zone width was 5.5, 5.5, 3.8 (start), 5.5, 5.2, 3.4 (centre), and 6.1, 5.5, 4.4mm (end) for the top, middle and bottom regions of the sections. Fig. 2a-c show general views of the three sections and Fig. 2d and 2e typical photomicrographs of the mid depth region of the section taken from the centre of the specimen.

A radiograph was also taken through the depth of the weld for a 25mm thick slice taken from the remainder of the specimen, see enclosed radiograph (A9911 section marked M to F and W11). No defects could be detected.

Continued/4

Mr. L. Werme,  
SKBF

Our Ref: AS/BCT/547.82  
1st September, 1982

---

### 3.2. TEST SPECIMEN W12

When the weld was repeated at 50mm/min (specimen W12) in the OFHC copper although penetration increased, so did the defect level see copy of radiograph (neg. no. 50892). Also top surface cavitation extended to 10-20mm. It was therefore concluded that for this size of specimen, at least, a welding speed of 50mm/min was too low.

Specimen W11 was considered to be our best result to date, but because of the heat build up effect, we began to wonder whether or not we were getting a true indication of penetration. It became obvious that we must carry out some thermocouple tests to deduce what size of specimen, and after what duration of welding time, the penetration depth could be assumed to be realistic.

Thermocouples were attached to the surface of the copper block as shown in Fig. 3. Welding was commenced 50mm from the centre of the block. This was done to simulate better the situation in circumferential welding where the heat sink always extends behind and before the weld pool. In addition a beam slope up time of 15 seconds was selected giving an expected full current condition 25mm after initiation. In practice for 106 x 106mm section material, penetration was achieved after 22 seconds and the temperature rise recorded was 110°C. In comparison, when the block dimension 'A' was increased to 212mm, 106mm penetration was achieved in 18.5 seconds (note slightly reduced time may have resulted from the fact that in this case a joint was being made, whereas the previous 106 x 106mm specimen test was strictly a melt run). On the other hand, for the large block the temperature rise was only some 5°C. It was therefore concluded that at a power of 150kV x 500mA and a welding speed of 100mm/min, 106mm penetration could be achieved irrespective of block size.

### 3.3. PHOSPHORUS DEOXIDISED MATERIAL; SPECIMEN W20

Multiple welds were made between slabs of 50 x 100mm<sup>2</sup> PDO material to build up a test specimen of comparable size to that of specimen W11. Finally weld (W20) was made using identical welding conditions. The radiograph taken perpendicular to the welding plane (see enclosed neg. no. 50891) showed a fine dispersion of microporosity but no major defects in the body of the weld (NB 'A' in this case depicts start of weld). This was also confirmed by microsections, see Fig. 4a-d. The microsections show a much higher level of microporosity than the OFHC material but the largest pore seen in the three sections taken (start, middle and finish of weld)

Continued/5

Mr. L. Werme  
SKBF

Our Ref: AS/BCT/547.82  
1st September, 1982

---

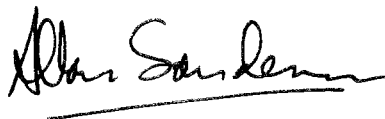
was only approximately 1mm in diameter. Radiographs taken through the depth of the weld in 25mm slices taken from the start (S) to middle (M) and middle (M) to finish (F), (see radiographs A9911 specimen marked W20) revealed only microporosity. The microporosity did however appear to be concentrated in semi-circular shells delineating the instantaneous freezing front positions, particularly at the start of the weld.

#### 4. SUMMARY

From the initial feasibility study carried out it appears that 100mm penetration can be achieved in copper with a power level of 150kV x 500mA at a welding speed of 100mm/min. Heat build up caused by use of this low welding speed results in a gradual increase in penetration but with apparently no adverse effect on the integrity of the weld. The OFHC copper welds made under these conditions are free from major defects, although some microporosity is evident. In comparison the microporosity level produced in the PDO copper is considerably higher than the OFHC copper but no major defects have been detected in the PDO welds made to date.

In conclusion it appears feasible to fabricate the canisters by EBW and we look forward to your final instructions for the simulated lid welds.

Yours sincerely,



A. SANDERSON (Dr)  
Head of Electron Beam Welding Section  
ADVANCED HEAVY SECTION PROCESSES DEPARTMENT

Encs:

4 radiographs

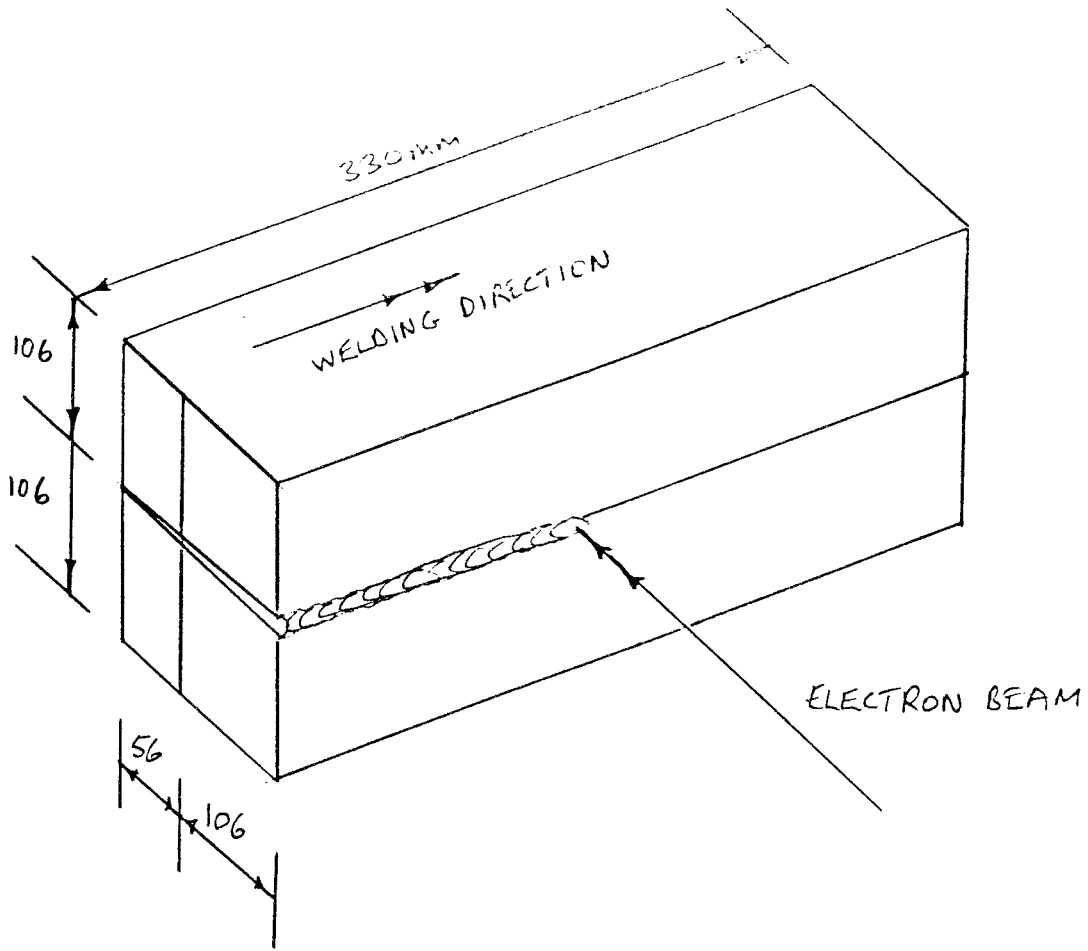
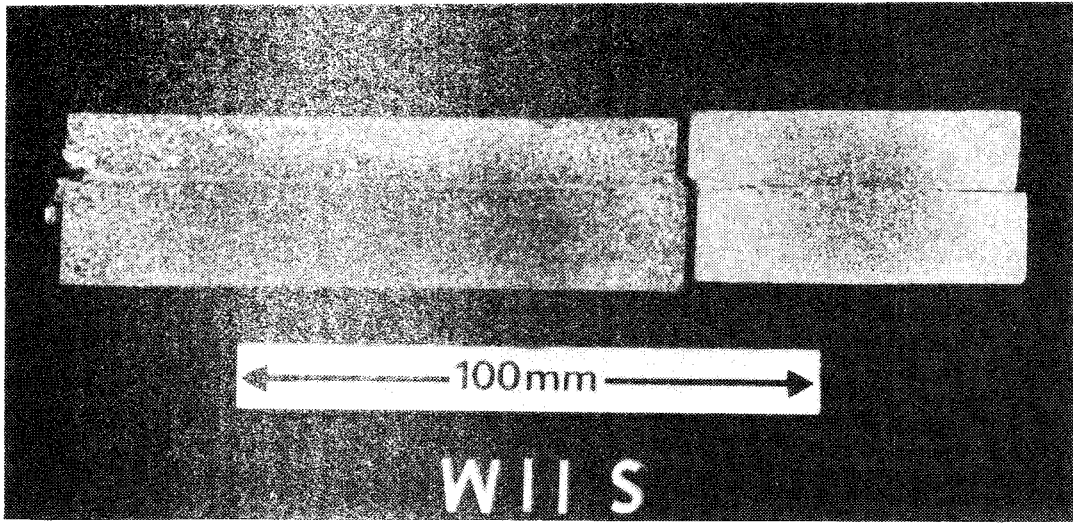
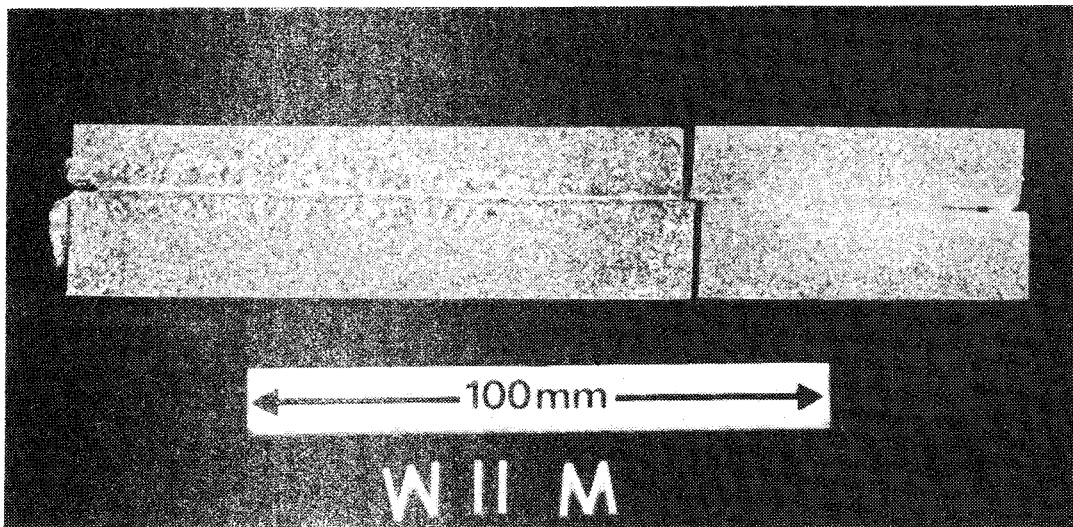


Fig. 1. Specimen configuration for W11, W12



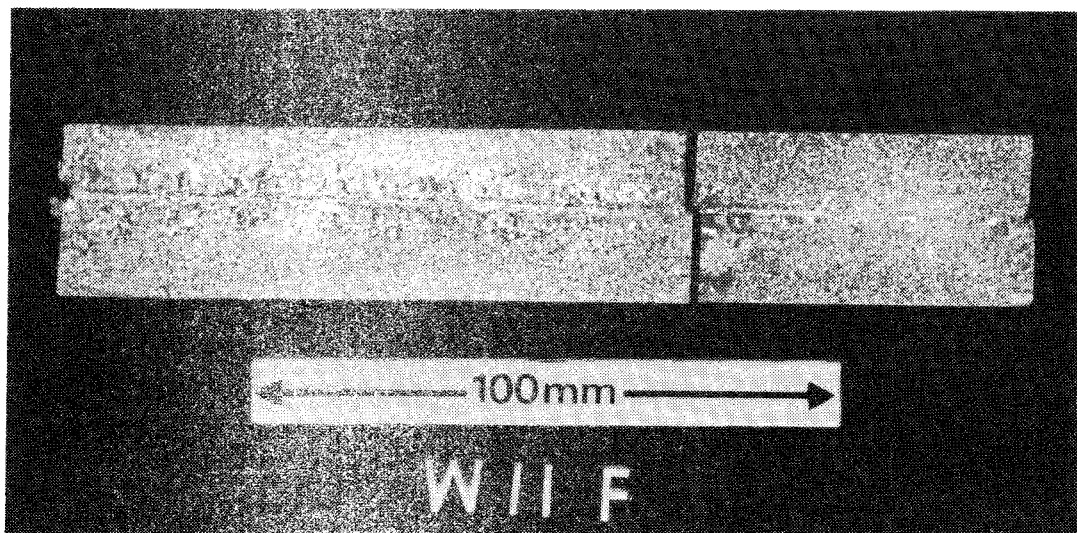
a)

50844



b)

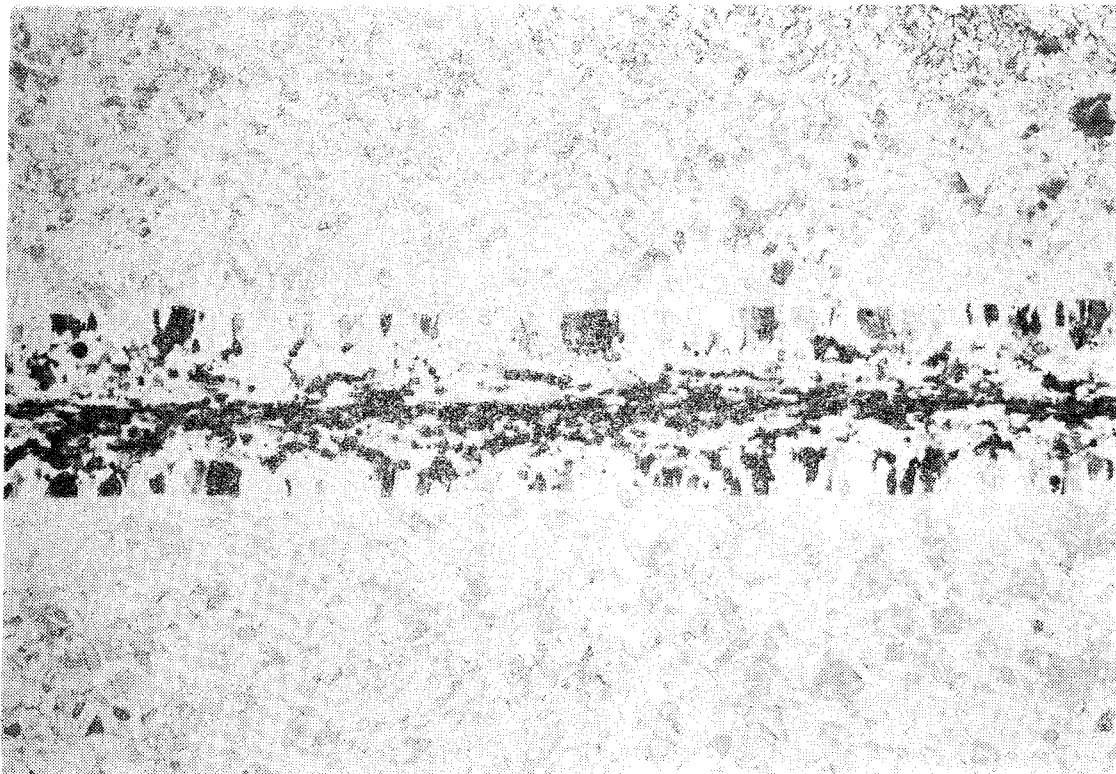
50846



c)

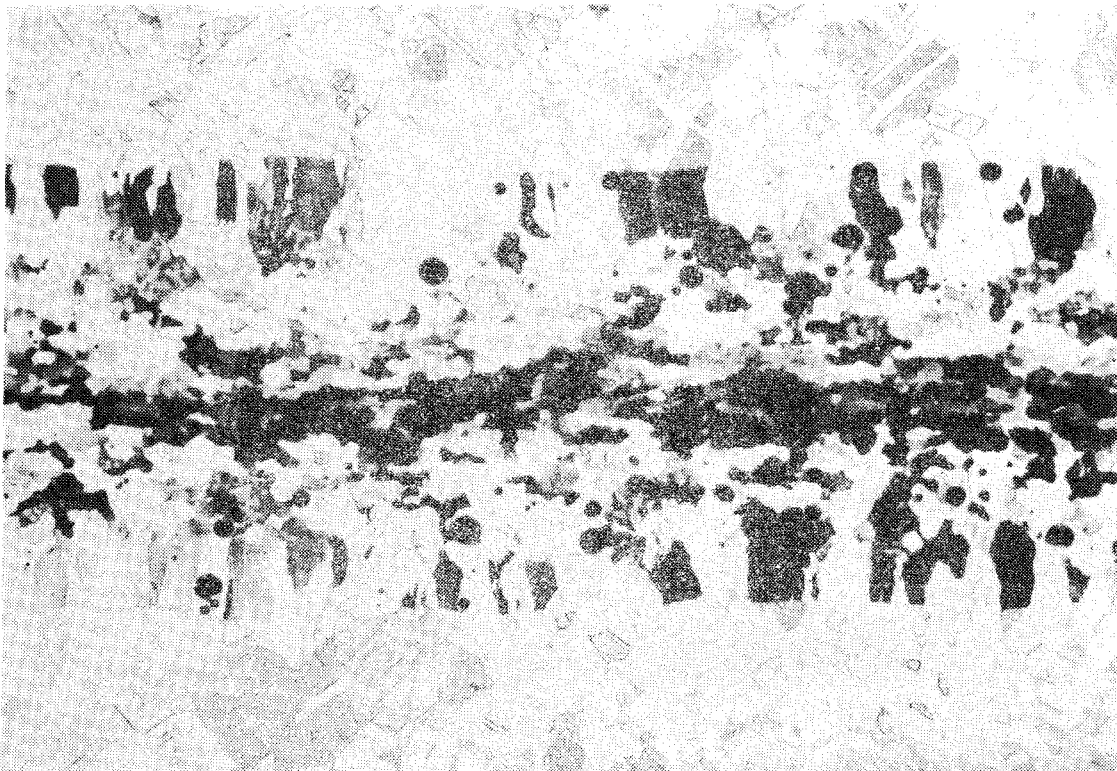
50845

Fig. 2. Transverse sections of OFHC specimen No. W11 showing a) 50mm after start of weld b) centre of weld and c) 50mm before end of weld.



d)

OS 2616



e)

OS 2615

Fig. 2 Continued. Photomicrographs showing structure detail in central region of OFHC specimen W11M d) x5 and e) x12

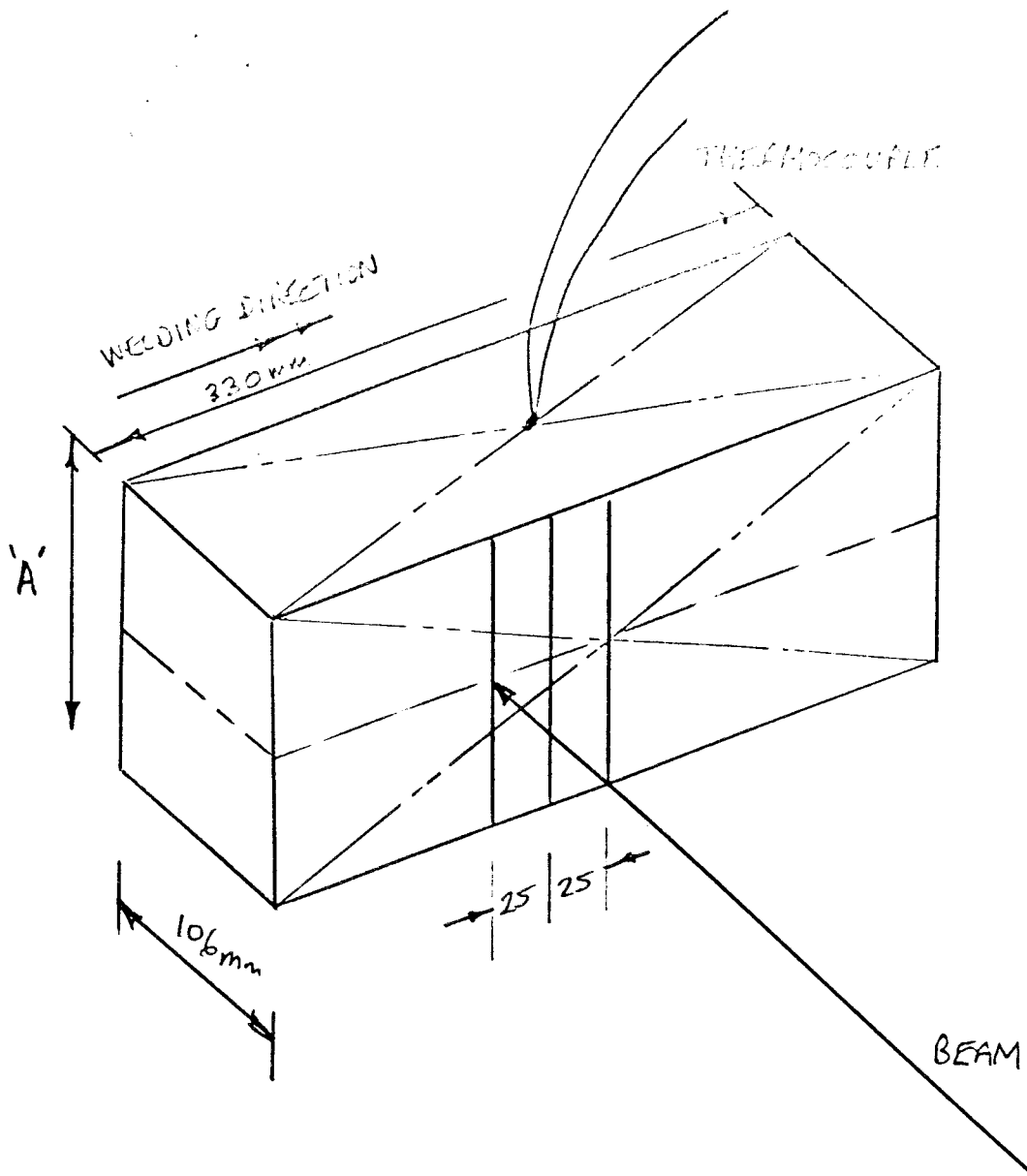
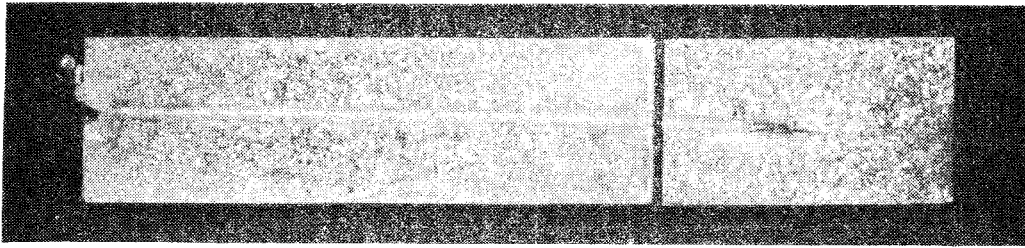
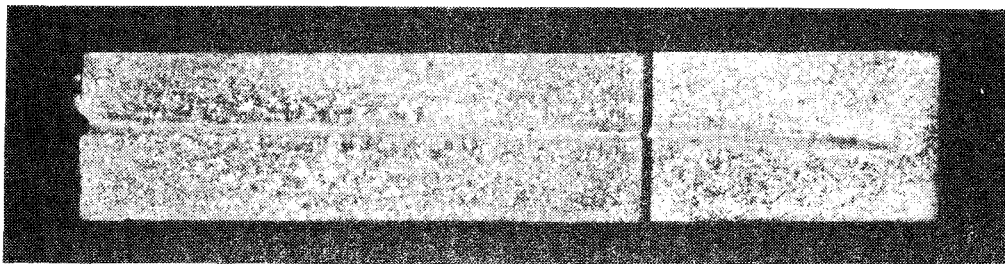


Fig. 3. Specimen configuration for beam penetration and surface temperature tests



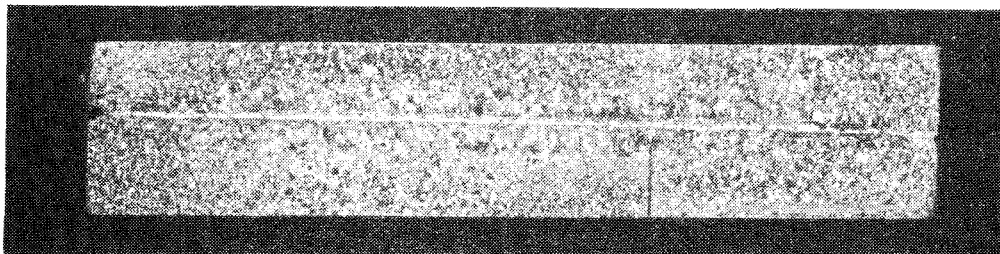
a)

50843



b)

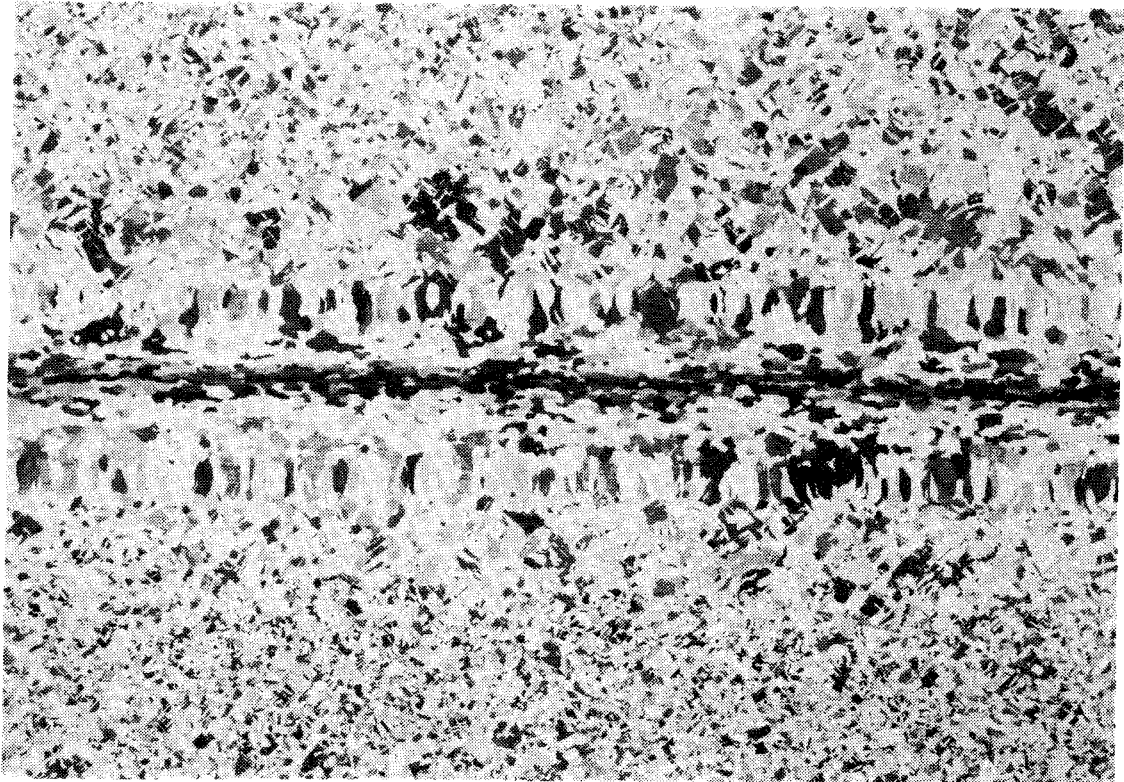
50841



c)

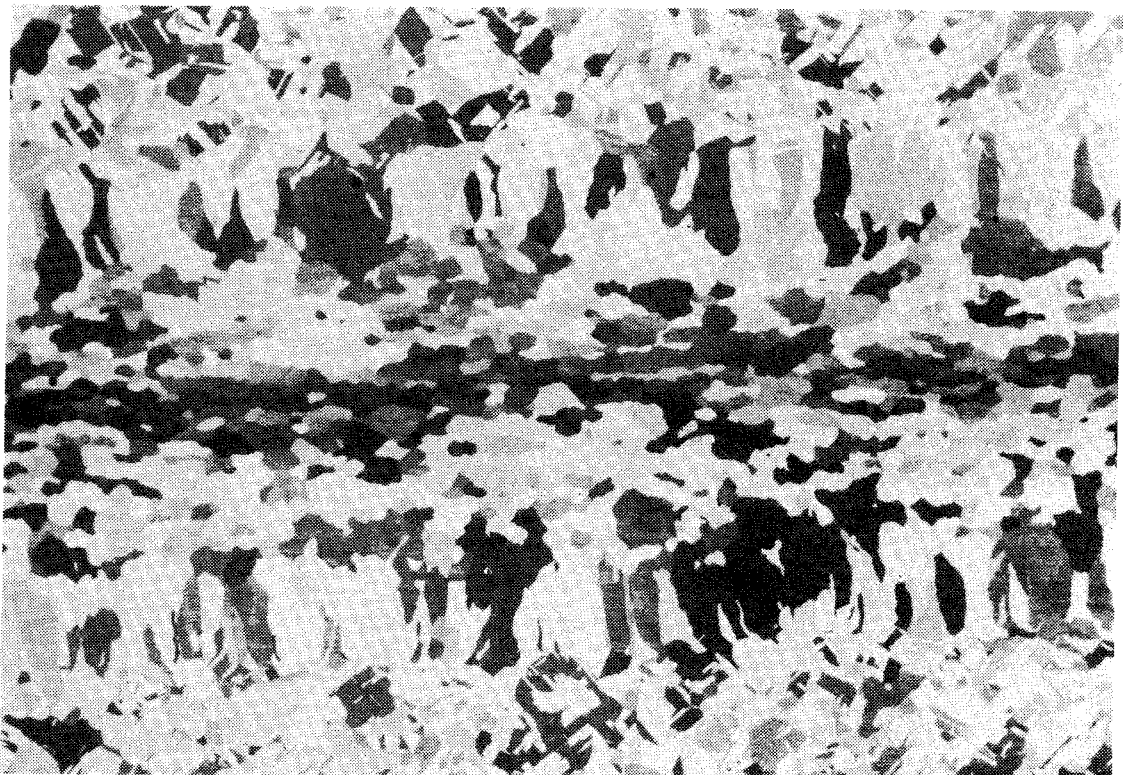
50842

Fig. 4. Transverse sections of PDO specimen No. W20 showing a) 50mm after start of weld, b) centre of weld and c) 50mm before end of weld. Magnification x0.75



d)

OS 2617



e)

OS 2614

Fig. 4. Continued. Photomicrographs showing a structure detail in central region of PDO specimen W20M d) x5 and e) x 12

# FEASIBILITY STUDY OF ELECTRON BEAM WELDING OF SPENT NUCLEAR FUEL CANISTERS - PHASES II AND III

By: A. Sanderson, T.F. Szluha and J.L. Turner

---

## 1. GENERAL INTRODUCTION

In the work reported earlier (see letter report 1st September, 1982, Our Ref: AS/BCT/547.82) an account was given of the development of welding conditions for 100mm thick OFHC and PDO copper in the form of bar stock. In the work reported here an attempt was made to establish suitable weld overlap and beam fade out conditions for the envisaged circumferential lid joints. For relatively thin components, that is with a wall thickness of up to some 50mm, sound EB welds can often be achieved by merely gradually decaying the beam current after the weld overlap has taken place. When thicknesses of the order of 100mm are involved, it has been found necessary not only to decay the beam current but also to slope-up the beam focus position. Much of the work reported here has been concerned with optimising the combined beam current and focus parameters. X-radiography perpendicular to the welding plane have been used as the primary means of assessing the merit of each approach tried, but since ultrasonics provides the only viable NDT technique which can be used on the canisters in practice, a good selection of the samples produced have been inspected by both means.

As far as can be ascertained, little or no work has been carried out on the ultrasonic inspection of EB welds in thick section copper using any of the accepted NDT techniques, so the investigation performed here breaks new ground in establishing methods and procedures for an unusual welding situation.

## 2. ELECTRON BEAM WELDING EQUIPMENT

All the work was carried out in The Welding Institute's 75kW EB1 (2m x 2m x 2m) machine equipped with a magnetic trap device. A working distance of 150mm was employed and all the welding was performed in the HV mode at a vacuum pressure of approximately  $5 \times 10^{-3}$  torr. A nominal accelerating voltage of 150kV was used throughout, but recent careful calibration of EHT has revealed that the actual voltage used for all this work and Phase I was 143kV.

## 3. MATERIALS

Linear welding trials were performed entirely on 50 and 100mm OFHC copper bar stock supplied from Outokumpu Oy to BS 3839:1965 and ASTM

F68-77. The 600mm diameter simulated lid OFHC copper components were also supplied by Outokumpu Oy and machined by Rauma Repola Oy.

#### 4. DEVELOPMENT OF FADE-OUT CONDITIONS

The standard copper block assembly used for the weld overlap and beam fade-out trials is shown in Fig. 1. A thermocouple was inserted in the centre of the upper block top face. The general welding procedure adopted was as follows:-

- i. joint tack welded at a current of 50 to 75mA;
- ii. blocks welded with beam current of 500mA (72kW);
- iii. blocks allowed to cool in vacuum chamber until temperature attained approximately 350°C;
- iv. Second pass commenced 50mm from end of block; beam parameters varied according to Fig. 2.

A UV recorder was used to monitor beam current and focus coil slope rates. This data was also checked and supplemented by manually noting the beam current and focus meter readings at set time intervals. Welds were subsequently sliced out and radiographed transverse to the joint plane.

Table I summarises the tests and results achieved using this approach. To commence, the beam current was decayed from 500mA to zero in 90 seconds with a fairly linear slope whilst maintaining a constant focus coil current of 1.400, see Table I run number 21 and Fig. 3. This gave rise to a steeply rising almost continuous train of root defects accompanied by medium sized rounded pores, Fig. 4. Also the weld top bead showed a badly undercut profile, the maximum depth of undercutting was some 13mm.

In an attempt to reduce the defect level, the beam focus was ramped up from 1.40 to 1.60A in sympathy with the decaying beam current, weld No. 22 Fig. 5. This would have the effect of drawing the focus closer to the top plate surface as the depth of penetration of the beam was reduced. In this case the focus ramp was linear (slope shape curve 5). The result of this exercise can be seen in Fig. 5. The defect and the undercut level were somewhat reduced and the root defects were less prominent although the chain was still almost continuous. For weld runs 21 and 22 the backing material was left on, but in subsequent runs the backing was removed to simplify cutting and radiography.

In the remaining tests of this series, the beam current fade out time was increased to 200 seconds. For weld numbers 46 and 47 the linear beam focus slope shape (curve 5) was retained but the focus ramp initiation was delayed, Fig. 6. The weld undercut was large in both cases Fig. 7 and 8, also the defects were larger and appeared in a greater quantity. An attempt was made to reduce the undercut on weld number 47 by using a defocussed 'cosmetic pass'. A beam current of between 50-80mA was tried on the first 200mm length with a 20Hz circular oscillation amplitude of 3mm. The beam was also defocussed

by setting a coil current of 1.40A. This unfortunately did not appear to be beneficial and in fact probably resulted in increased undercut. For the last 110mm of weld the oscillation amplitude was increased to 9mm. On the surface, this appeared to fill the undercut but radiographs indicated the generation of a large area of defects, Fig. 8.

Weld number 48 was made with identical conditions to number 47 except the focus slope shape was modified to a convex form (slope shape 9), Fig. 9. This approach appeared to improve the depth of weld undercut but the train of root defects was still quite prominent, Fig. 10.

At this stage it was suggested that beam current ripple, which is known to amount to some 8% (peak to peak) from the supply used for the work could be partly responsible for root defect formation. The theory was that fluctuations in beam current could cause a stitching action and adverse metal flow conditions in the weld cavity. To test this an alternative EHT supply which has a ripple level of approximately 2% was tried and weld number 49 made with nominally identical conditions to number 48. This showed no significant improvement, Fig. 11 of Fig. 10.

For weld numbers 52 and 53 the beam focus fade-out time delay ( $T_4$ ), after the initiation of beam current decay was altered, see Table I, and Fig. 9.

With a time delay of 40 seconds (weld number 52) the weld root defects were not as continuous. However, when this time was reduced to 20 seconds, although the root defects were almost eliminated, large rounded pores occurred just prior to loss of penetration through the 100mm thick plate and the top surface undercut reached a maximum of some 24mm. All of the tests listed in Table I were made with no beam oscillation except for run numbers W46 and W47 in which a Y amplitude of 0.5mm was applied at 140Hz.

#### 4.1. Control of Root Defects

In parallel with the standard test block programme described above a second programme of development was run. In this the penetration depth was generally limited to less than 100mm by holding the beam current constant, so that the effect of various beam control parameters could be studied. Without special techniques the top of the penetration finger tends to be very narrow and pointed. Particularly in high conductivity materials such as copper the liquid metal freezes prematurely. There is insufficient time for the keyhole to be completely filled with liquid metal as the beam progresses along the joint line. The results are as seen for example in Figs. 4 and 5, i.e. a train of 'cold shut' defects and associated pores.

In principle it ought to be possible to prolong the time for which the metal remains molten to facilitate filling. To this end various techniques were explored.

#### 4.1.1. Castellated Y Oscillation Pattern

##### 4.1.1.1. Effect of Y Oscillation Amplitude and Focus Position

In the first series, a castellated Y (across the joint line) beam oscillation pattern was tried. This effectively splits the beam into three beams. Oscillation amplitude and focus position were varied as shown in Table II. The root defects as indicated by transverse radiographs were rated in severity using an arbitrary scale of 0 to 10 where a value of 0 would represent a continuous train of large pores extending fully depth of the penetration finger. A value of 5 indicates an almost continuous train of prominent defects some 20mm deep and a value of 10 represents complete freedom from defects. To commence a beam current of 300mA was applied (specimen number 23A-C) this gave rise to intermittent full penetration of the 100mm thick block making defect assessment difficult. Therefore, in subsequent runs the current was reduced to 200mA which generally gave a penetration depth of some 70mm.

From Table III, it can be seen that in this case increasing oscillation amplitude has a deleterious effect particularly at focus coil current levels of 1.46 and 1.48A, but at 1.50A this effect is less significant. Also the results indicate a general trend of improvement as the focus coil current was increased. A focus coil current of 1.50A corresponds to a beam focused approximately 50mm below the top surface. Remarkably run 24A was apparently almost completely free of defects, but a section taken of this weld indicated a root defect extending for a depth of some 7mm albeit with a width of less than 0.3mm. Once again this section indicated the need to increase the width and roundness of the tip of the penetration finger, Fig. 14. On the other hand, although microsections of run numbers 23E and 25E showed some general increase in fusion zone width, the penetration tip width was still too narrow and sharp.

##### 4.1.1.2. Effect of Frequency

In this test series frequencies of 14, 140, 1400 and 2800Hz were used at Y amplitudes of 4mm and 2mm, Table III. Generally the defects were more evident in run number 26 made with the higher oscillation amplitude. Also at the lowest frequency tried, i.e. 14Hz, very large clusters of defects were produced when the amplitude was 4mm. The best results were produced at a frequency of 140Hz and for the higher amplitude the defects were significantly shorter although of greater width. Sections taken through runs 26B and particularly 27A showed three distinct penetration fingers extending over a depth of some 15mm in the latter case. Evidently there was insufficient residual power in the 'three' beam cores to cause merging of the separate fusion zones, Fig. 16. In the former case (26B) the penetration finger tip shape was broader, Fig. 15, but there was a localised region of cold shuts and pores.

In a subsequent test (run 28) the Y-oscillation amplitude and frequency were fixed at 4mm and 140Hz respectively and focus levels of 1.4, 1.45,

1.50, and 1.55 amps were applied. All welds showed good bead profile but the defect level varied as shown in Table IV.

#### 4.1.2. Triangular Y Oscillation Pattern

In this test series the Y oscillation amplitude was fixed at 2mm and four different frequency levels were tried, Table V. The overall effect was to produce very fine, but deep defects. The best results were achieved at a frequency of 70Hz.

#### 4.1.3. X-Y Raster

In a further attempt to broaden the fusion zone, X and Y oscillations were combined to produce a 'block heat source' or raster, Table VI. For a 2 x 2mm<sup>2</sup> raster the defect level was low but as raster X length was increased, very deep defects appeared. When the raster size was extended to 5 x 2mm<sup>2</sup> the weldpool became unstable giving rise to 3-4mm full penetration depth cavities separated approximately by only a cavity width.

#### 4.1.4. Figure of Eight Pattern

##### 4.1.4.1. Effect of Amplitude

A figure of eight lissajous pattern was applied with the long axis coincident with the jointline, Table VII. Once again, gradually increasing oscillation amplitude was seen to progressively increase the severity of the defects.

#### 4.1.5. Very High Frequency Deflection

Recently a special purpose 236kHz concentric circle pattern generator has been produced for weldbead and spatter control. It was thought that this might possibly provide a more diffuse spread of the heat source. The parameters used are given in Table VIII.

Because of the need to fit additional deflection coils it was necessary to increase the working distance. A focus coil current of 1.34A was then used to provide comparable focus conditions to previous tests. Although this approach was only briefly explored, no major improvements were noted.

#### 4.1.6. Increased Welding Speed

In these trials the welding speed was increased in steps as an alternative means of reducing penetration after the weld overlap. A focus coil current of 1.4A was adopted, Table IX. The penetration depth at 500mA was approximately 100, 90, 70 and 60mm at 1000, 750, 500 and

250mm/min speeds respectively. The defects in this case were quite severe, consisting of virtually continuous trains of large pore clusters.

Later the concept of increasing welding speed combined with decaying beam current was studied. This, however, showed no particular promise; in the region where the speed was at 250mm/min for a beam current range of 156 to 67mA, an almost continuous train of defects were detected between a depth of 50mm and 10mm.

#### 4.2. Discussion

A fairly wide range of oscillation patterns and amplitudes has been explored. It is evident from the results that magnetic deflection of the beam influences the way in which the weld metal flows and solidifies in the region of the penetration tip. Large deflection amplitudes however, generally have a deleterious effect, resulting in weldpool instability and gross cavity formation. No particular benefit appeared to accrue from the use of high or low frequency oscillation and generally the best results were obtained for frequencies of approximately 140Hz, with simple Y oscillation patterns. Some benefit has been seen with certain deflection patterns but a pattern has yet to be established which produces a rounded penetration finger with no cold shut defects. On the other hand, the combination of patterns tried in this work can be, by no means, considered exhaustive.

Regarding the use of increasing welding speed to effect fade-out, this appeared to aggravate the root defect problem even when combined with normal beam current fade-out. In contrast focus position apparently has a fairly large effect on defect formation and providing the beam current fade-out rate is relatively slow the defect occurrence can be minimised if not eliminated.

In view of these difficulties it was decided that beam oscillation technique had not shown sufficient improvement to use them on the first simulated lid weld, so the beam and focus fade-out conditions similar to run number 52 Table I were adopted.

#### 5. ELECTRON BEAM WELDING OF SIMULATED LID WELD

The configuration of the simulated lid weld is shown in Fig. 17. Since it was convenient to use 100mm copper plate the lid comprised a disc and a ring. The disc represented the neck of the lid and provided the backing material. For ease of welding the component was inverted and rotated around a vertical axis. A surface welding speed of 120mm/min was selected so that the speed at depths of 50 and 100mm was 100 and 80mm/min respectively. The joint interfaces of the components were cleaned with a fine emery wheel and degreased immediately prior to welding. The assembly was placed on a 58mm thick steel base plate and a 20mm diameter steel stud with a 28mm thick steel top plate were used to clamp the components together. Thermocouples were embedded in the surface of the copper ring which simulated the canister wall, Fig. 17b.

The full welding parameters are given in Table X. Before commencing the main weld the joint was tack welded at 75mA. The first tack weld was made 60mm long followed by a 120mm long tack placed diametrically opposite. The third tack weld, 120mm long, was placed at 90° to the start of the first two tack welds followed by a continuous full revolution tack started diametrically opposite the third tack. This approach was adopted to avoid any possibility of the joint gap opening up.

A complete video recording of the welding was made, and a continuous record of temperature changes. Welding progressed satisfactorily for the first 695 seconds. At this point the power supply inexplicably shut down. The component was reversed for approximately 30mm and the beam 're-faded-in' after a total delay of 2mins. After a further 20 seconds of welding a second supply 'shut down' occurred some 10mm after overlapping the first. The weld was re-initiated from this point after a subsequent delay of 2mins and successfully completed; no further attempt was made to repair the damage caused by supply 'shut down'. Fig. 17b indicates the orientation of the various events.

Figure 18 shows a general view of the welded lid. As with trial welds there was a tendency for the weld metal to pour out. The average weld undercut was 3 to 4mm.

Figure 19 shows the temperature data produced during welding. To align the unfocused 1.400A beam with the joint it was necessary to use approximately 40mA. This caused a small initial temperature rise. Tack welding produced a family of 4 peaks on the thermocouple plots raising the peak temperature to 90°C. During the main weld the maximum temperature attained was 525°C, but after 10 minutes equalisation of heat by conduction had dropped the average temperature to less than 400°C. This is in good agreement with the theoretical prediction. The result of the power supply 'shut down' difficulties can be seen as a double inflexion and delay in peaking, of the thermocouple no. 4. After removal from the traverse the lid components were allowed to cool naturally in air. Residual stress measurements were carried out by Dr. R.H. Leggatt (see letter RHL/CFH/0665.83 (LD 22967) and subsequent report).

The weld beads were then removed by machining and it was found necessary to reduce the radius by 5.8mm to clean-up the entire periphery (apart from that caused by the fade-out region and 'shut down' defects). After ultrasonic tests see section 6, and further residual stress measurements the component was then cut into four quadrants as indicated in Fig. 17b. The cutting axes were rotated approximately 13° with respect to the start to ensure the entire fade-out region was contained in one quadrant. One face of quadrant BOC was polished and etched and then returned to SKBF for further ultrasonic tests. Quadrant AOD was retained in tact for further residual stress measurements and the welds in quadrant AOB and DOC were cut out longitudinally in 27mm slices for X-ray examination. Transverse metallographic sections were taken later as described in section 8.

## 6. ULTRASONIC INSPECTION

### 6.1. Introduction

There were three main considerations in applying ultrasonic techniques to the 100mm thick lid weld, viz:-

#### a) Acoustic Attenuation

The attenuation of the ultrasonic waves in copper is much higher than that of steel (for example), and has varied widely from specimen to specimen in this project. This has caused correspondingly large variations in the sensitivity of the ultrasonic probes to defects located within the specimens. In addition, if the attenuation is too high then a visible reduction in the mean frequency of the returning pulse occurs (particularly for the higher frequency probes used) which must be taken into account in selecting the flaw detector bandwidth setting.

#### b) Choice of Equipment and technique

The high ultrasonic attenuation exercises a considerable influence on the choice of probe crystal diameter and frequency. It also governs whether the ultrasonic inspection should be conducted with the probe in contact with the specimen, or in an immersion tank with a water path between the probe and specimen surface. Where possible, the latter technique was preferred, since it could be performed on our automatic C-Scan facility. In addition, it reduces problems arising from coupling variations between probe and specimen which are difficult to ignore when performing a manual contact scan.

#### c) Defect Sizing

To assist defect sizing a solid copper test block of dimensions 330 x 105 x 100mm was made with four 5mm deep flat bottomed holes of diameter 13, 8, 4 and 2mm drilled into one of the 330 x 105mm<sup>2</sup> faces. It transpired that the attenuation in this block was so high that it was only barely possible to detect the 2mm hole with the largest immersion probe used (a Panametrics 2.25MHz probe with a 38mm diameter crystal). When probes with such large crystals are used, they produce beams which are considerably larger in diameter than the defects themselves, which makes sizing of the defects from the C-Scan plots extremely inaccurate. This problem was not made any easier by the fact that the main defects apparent (i.e. those in the beam fade-out region of the welded specimens), consisted of closely-spaced collections of pores and cavities. This meant that several of these defects would appear within the area of the beam, thereby making discrimination difficult.

## 6.2. Results

### 6.2.1. Welds in Copper Blocks - 100mm Thick

As related during the visit by SKBF representatives to The Welding Institute on 9th December, 1982, it was apparent that, on the basis of the specimens (W21 and W22) inspected up to that point, immersion scanning did not appear to provide the most promising prospect for success. The majority of the ultrasonic scans had subsequently been performed manually with probes of crystal diameter 10-15mm and frequencies of 1.25, 2.5 and 4MHz used in contact with the specimens. In all cases, the weld zone was 100mm below the scanning surface. Higher frequencies (e.g. 4MHz) offered greater resolution owing to reduced beam divergence, but care had to be taken to ensure that sensitivities were not too low due to the high attenuation encountered.

Of the welded specimens produced thereafter, two (W46 and W47) were inspected manually using a KB Aerotech (Gamma series) 19mm diameter, 2.25MHz probe. After these had been sectioned and X-rayed, the sections (about 20mm thick) were placed in the immersion tank and the same probe used to produce C-Scans. The results obtained by the two techniques showed a fair amount of agreement, with the fade-out defects being clearly apparent in both cases.

On the whole, the X-radiographs showed all the fade-out defects detected ultrasonically, but made the detailed structure and size of the defects much more clearly apparent.

The fade-out defects nearly always registered as the strongest indications in the case of both ultrasonic and X-ray techniques. However, some ultrasonic indications (albeit at a somewhat lower level) appeared outside the fade-out region that were not apparent on the radiographs.

### 6.2.2. 600mm Diameter Simulated Lid Weld (Specimen W55)

The thickness of both the cap and ring were 100mm thick at the circumference, and the depth of the welded zone was 100mm.

At first it was decided to perform a contact scan from the underside of the ring (Fig. 20) using the KB Aerotech 19mm diameter, 2.25MHz probe driven by a Sonic Mark IV Flaw Detector. A rapid scan all round the annular surface of the ring showed that the majority of defects were concentrated between the 'fade-in' point and the end of the fade-out zone, that is in quadrant AOB of the ring (Fig. 17b). Hence it was decided to start detailed inspection on this portion of the ring. Fig. 21 shows the results of this, with the fade-out defects clearly shown in a spiral band between the inner and outer diameter of the ring.

During the course of the inspection it was discovered that this particular copper specimen had a much lower acoustic attenuation than previous testpieces. Consequently, it seemed that this specimen might be a good candidate for immersion testing.

The specimen was set up in the immersion tank to enable scanning to be carried out with the same probe positioned such that there was a 90mm water path between the transducer element and the surface of the cap (Fig. 22). Scanning through the cap meant that it might be possible to view any defects arising from electron beam penetration beyond the weld zone into the parent material of the cap itself. The results of this scan are shown in Fig. 23.

It will be noted that the location and extent of the fade-out defects agrees closely with that apparent in Fig. 21, despite the fact that scans were conducted from opposite sides.

The arrowed point on the C-Scan plot indicates that the area from which the largest signal was observed. The darkest level of grey represents regions where signal amplitudes were no more than 6dB below the maximum signal. Similarly, the two following lighter shades of grey indicate successive 6dB drops in intensity. Thus the C-Scan displays an 18dB range of signal amplitudes.

Clearly shown on Fig. 23 are the fade-out defects (and on the other side of the ring) a radial defect arising from shut down of the beam. Since the test cap consisted of an assembly of two components (Fig. 22) the interface between them obviously hampers the penetration of ultrasound into the lower part of the cap. Therefore, it would be unreasonable to expect a representative scan of this particular region of the fusion zone. However it was found that if scan sensitivity was increased by, say, 6dB (Fig. 24), then areas of the region within the cap became visible.

Despite the relatively poor resolution of the transducer used in the C-Scans presented here, it is still possible to obtain some estimate of the size of the major defects observed. Considering the parameters of the particular probe used, one can calculate the angular divergence of the beam in a zone where the radiated intensity is within 6dB of the maximum value (which is presumed to be along the axis of the beam). This implies that the beam has a diameter of approximately 14mm in the region of the weld. Since this is of the same order as the width of the darkest band of grey observed in the fade-out zone, then it is reasonable to suppose that the dimension of the defects (along an axis perpendicular to the band) must be a small fraction of the width of the beam, i.e. of the order of 1-2mm or less. This is borne out by the X-radiographs obtained showing fade-out zone defects in the previous specimens.

#### 7. X-RAY EXAMINATION OF SIMULATED LID WELD (SPECIMEN W55)

Longitudinal slices were cut from the welded lid quadrants AOB and DOC. X-radiographs of these regions are shown in Fig. 25a and 25b reproduced at X0.7. The 'shut down' defects Fig. 25a appear as two needlelike holes, in one case penetrating the entire wall thickness to a total depth of nearly 160mm. Also associated with this region are a series of pore clusters which could possibly have been caused by 're-fading-in' the beam and excessive local heat input as a result of the over-lapping weld. Fewer defects occur away from this region. In the fade-out region,

Fig. 25b, a string of defects was detected, marking the position of the root of the gradually reducing penetration depth. However, the number and severity of defects was at least as good as in the linear development trials (see fig. 12, W52). Just prior to loss of penetration of the 100mm section a group of more randomly dispersed defects occurred. Fig. 25b also allows a comparison to be made of the penetration depths during the early stage of welding with that after one complete revolution. In the cold state a depth of some 135mm was achieved whereas this increased to nearly 200mm in the hot overlap region.

## 8. METALLOGRAPHIC EXAMINATION

In order to further clarify the nature of the defects revealed by ultrasonic and X-ray techniques, four transverse metallographic sections were taken as indicated in Fig. 26a and b. Three sections were taken of the fade-out region (specimen numbers 55A/1, 55A/2 and 55A/3) where defects were clearly visible on the radiographs and one section in an apparently sound region (specimen number W55B/1, Fig. 26b). Macrographs of these sections are shown in Figs. 26a to d. The large defects in specimen 55A/1 were mainly as predicted but a string of small pores extending from a depth of some 10mm were found running along the fusion zone boundary in the upper region of the weld, Fig. 26b. No significant defects were revealed in specimen 55A/3, Fig. 26c, apart from the expected root pore shown in the radiograph.

The apparently sound weld in specimen 55B/1 was indeed found to be completely free of defects, Fig. 26d. The position of the four sections have also been marked on the C-Scan image and the radiograph.

## 9. GENERAL DISCUSSION

Good progress has been made in the development of welding conditions for 100mm thick copper and it has been shown by linear weld test blocks and the first simulated lid weld that the defect level can be minimised by the correct combination of the beam current and focus fade-out rates, curve shape and time relationship. However, in spite of substantial efforts to establish a beam oscillation technique to eliminate porosity, no major breakthrough can be reported. Oscillation frequency and pattern affect porosity formation but the key to complete weld pool control has not yet been found.

At one stage it was thought that the EHT power supply characteristics could be affecting the defect problem but no significant difference was found between welds made using supplies with 2% and 8% peak to peak beam current ripple. Similarly the use of increased welding speed to effect penetration fade out was disappointing.

Nevertheless the first simulated lid weld attempted (specimen number 55), was at least as good as the previous trials except in the region where power supply shut down occurred. Fade-out defects consisted of a discontinuous series of discrete holes with a typical depth of less than 10mm.

Comparing X-radiographs and microsections with the ultrasonic scans, it is apparent that the latter technique in its present form gave poor resolution and it was only possible to obtain a rough estimate of defect size by estimating the beam width. Another method (untried here owing to lack of a satisfactory reference reflector in a test piece of similar properties to that of the specimen) is to size defects according to the received signal amplitudes, the so-called DGS method.

However, neither of these methods were well suited to the inspection situation discussed here, since the discrete defects were not widely separated, but were considerably closer together than the ultrasonic beam widths involved. This meant that the defect indications overlapped to create the impression of larger defect zones than were actually present. This also meant that it was difficult to decide whether the fade-out zone defects, for instance, were continuous, or closely spaced and discrete.

In addition, the signal peaks apparent to one side of the shut-down defects (Fig. 24) tend to blend into the fluctuating background signal observed here, thereby making location and orientation of any defect indication difficult to discern. The range of sensitivity used in Fig. 24, tends to create the alarming impression that there are small defects throughout the entire fusion zone as evidenced by the background signal.

In reality, the microsection through the region indicated in Fig. 24 contained no significant defects, whilst the microsections taken through the fade-out region and the X-radiographs revealed discrete non-continuous defects. The small defects observed in the vicinity of the shut-down defects, see Fig. 25a, appear to coincide with the signal peaks apparent to one side of the shut-down defects as displayed in Fig. 23.

Some discussion of the probable origin of the fluctuating background signal observed in Fig. 24 is now in order. This became even more clearly in evidence when the sensitivity was increased by the maximum available amount of 10dB above that in Fig. 23. A similar background echo was observed in the welds of previous copper specimens, and as a rule, did not appear to emanate from defects that were visible in the radiographs. One explanation is that the background echo could result from changes in the orientation of grains in the weld zone, and variations in their size relative to the grains in the surrounding material. Since the fluctuations in the background occur at a considerably lower level (20dB or more) than those from the main defects, it does not in any case appear likely that defects in this region (if any) represent anything of the same order of severity as those arising from fade-out and shut-down.

In addition, substantial differences have been noted in the attenuation of the ultrasonic signal for the simulated lid material and the bar stock material. This factor could well have an important bearing on the type of ultrasonic technique (i.e. contact or immersion) to be employed for canister inspection in practice. The lid material used in the present trials has been shown to be well suited to immersion

C-Scanning. Indeed it may be necessary to closely specify the manufacturing procedure of the canister (particularly the lid) in order to facilitate ultrasonic inspection of the weld.

To further improve the resolution of the defects as seen on the C-Scan, ultrasonic transducers with narrower beams need to be used to accurately resolve and size the small defects present in the fade-out zone. One would require the beam in the region of the weld to have a diameter of the same order as the defect size (i.e. 1-2mm). However, the high attenuation of the copper and the depth of the weld zone below the surface imply that such a stringent requirement could not be met by using normal commercially available ultrasonic transducers. Nevertheless, preliminary studies undertaken in the NDT Research Section have shown that beam widths can be reduced considerably over large ranges by acoustic focussing techniques.

There is no doubt that the beam fade-out region, as with other thick wall circumferential vessel EB welds, is the most critical part of the welding procedure. The defect level commonly achieved may not be considered tolerable since pores and cold shut defects in close proximity might lead to premature corrosion of the vessel wall. On the other-hand it is likely with further refinement of the EB welding process that the defect level could be reduced. Alternatively, after the overlap, the weld could be continued into the canister lid in a helical fashion before fading-out the beam current. This would have the effect of transferring the fade-out defects into the solid lid component. There would still of course be a series of root defects spiralling outwards on an upward helical path, but the potential corrosion paths would be greatly extended. Practically this approach is attractive but again careful consideration would need to be given to the NDT procedure and acceptance standards since defects would appear over a wide range of depths measured from the upper lid surface.

Regarding beam power requirements it appears that 72kW is just sufficient to achieve adequate initial penetration and a sound weld at a mid-thickness welding speed of 100mm/min. For the first lid weld, as the weld progresses, maximum penetration increased from 135 to 200mm. It is not expected that the beam power requirement will exceed 100kW for the full scale canister, although the maximum temperature rise will be substantially less than 400°C a distance of 100mm from the weld.

The possibility of interruptions in the welding process leading to defects, such as those in the first simulated lid weld, must be faced. The magnetic trap device used in this work is well proven as a means of preventing vapour from entering the electron gun but power supply shut-down can still occur due to, for example, dust particles entering the upper gun column during filament replacement. In the case of the supply shut-down events which occurred during the first simulated lid weld it is not clear what was the exact cause, but there was no clear evidence on the UV record or from the video recording to suggest that the gun had discharged. One possibility is that the current-overload circuit of the EHT supply malfunctioned. Finally, it can be mentioned that good progress has been made with repair techniques and these will be covered in the next report.

### 9.1. Practical Considerations of Electron Beam Welding Full Scale Canisters

It is currently proposed that the canisters would be 4.5m in length with a diameter of 0.8m. With a copper wall thickness of 100mm, the overall weight of the vessel including lead and spent fuel element would be in the region of 22 tonnes. So far it has been demonstrated that a simulated lid of 100mm thickness can be welded by electron beam although it must be admitted that further refinement of the process technology is required to achieve the necessary high weld integrity.

On the other hand, the question must be asked - what is the practicality of welding a full scale canister? The canister dimensions do not present any outstanding difficulties; electron beam welding equipment already exists which can house much larger components. Similarly, the design of suitable mechanical manipulation equipment would not be expected to create any particular difficulties. It is important that the canister axis is maintained vertical to facilitate welding and this fits in well with the preceding processes such as lead filling.

The canister could either be housed in a suitably tailored fully enclosing vacuum chamber or a local vacuum enclosure formed around the lid region. In the latter case, however, careful consideration would need to be given to the vacuum sealing means applied to the vessel wall, since heat and radiation might limit the life of the sealing material. For a fixed seal it would be necessary to rotate the electron column around the canister as for example is currently practiced in offshore J-pipe laying EBW equipment[1,2]. Alternatively a sliding seal arrangement could readily be devised in which case the heat source would be fixed whilst the canister was rotated.

Fully enclosing the canister in a vacuum chamber would probably simplify sealing arrangements and with a fixed external electron column it would only be necessary to rotate the canister. This could be done by gripping the outer wall in the region below the joint line. Of course, since the canister is very long, steadies or a lower central bearing would have to be included to ensure smooth axial rotation. However, there is no doubt that vacuum and electron beam technology is currently sufficiently advanced to enable a viable equipment to be designed and built.

Regarding the heat sink effect, it would appear that a 100kW beam would be sufficient to achieve in excess of 100mm penetration irrespective of vessel size, but there is a need to carry out further work to verify present indications.

## 10. CONCLUSIONS

1. Good progress has been made in the development of beam fade-out conditions but it is still not possible to completely eliminate root and cold-shut defects.
2. The first simulated lid weld in 100mm was successfully completed apart from two unexplained supply shut-down occurrences.

3. Beam penetration at 72kW for a mid-thickness welding speed of 100mm/min was some 135mm initially, rising to a maximum of 200mm towards the end of the weld.
4. The maximum temperature recorded for the lid components, 100mm from the weld was 525°C, but the temperature fell to below 400°C, 4 minutes after the welding was completed.
5. The present welding procedure leads to an average undercut level of some 4mm but in the beam fade-out region the maximum undercut reached approximately 8mm.
6. Automated ultrasonic C-Scan has been shown to be useful in detecting and displaying defects, but some problems still remain with defect sizing.
7. The OFHC lid copper supplied by the Outokumpu Oy appears to attenuate ultrasonic signal far less than the bar stock supplied by the same company. This is undoubtedly related to the manufacturing processes involved in the production of the two types of specimen.
8. The design and manufacture of an electron beam installation capable of the handling the proposed full scale 4.5m x 0.8m Ø canister is currently technically feasible.

## 11. SUGGESTIONS FOR FUTURE WORK

There appear to be several remaining areas which require more research and development effort. These can be listed as follows:-

1. Further refinement of beam fade-out techniques to reduce defect levels.
2. Study of effect of heat sink size on beam power versus penetration.
3. Continuation of the development of repair procedures (this is already underway and will be reported on in the near future).
4. Investigation of the effect of copper grain structure on ultrasonic attenuation. This, in turn, needs to be linked to the manufacturing processes involved in material production. In the final analysis, a range of acceptable attenuation values for the ultrasonic test procedure adopted would have to be specified.
5. Further development of the ultrasonic transducers to improve resolution of defects. This would be an extension of the work (on acoustic focussing techniques) mentioned in section 6.

12. REFERENCES

1. BRUNO DE SIVRY, SUDREAU, G. 'A new concept for pipelines : electron beam welding', paper OTC 4101, pp 299-303, 13th Annual Offshore Tech. Conference, Houston Texas, May 4th-7th 1981.
2. SUDREAU, G., BRUNO DE SIVRY, ANSELME, O.R. 'Electron beam weldability for deep sea pipelines' Paper OTC 4102, pp 311-316, 13th Annual Offshore Tech. Conference, Houston Texas, May 4th-7th 1981.

.....

TABLE I. Beam Current Overlap Weld and Fade-Out - Standard Test Block Data and Results

Weld No.	Beam Current Time Periods (secs)			FOCUS				Maximum Top Bead Undercut (mm)	Defect Description	
	Time Periods (secs)			Slope Shape No.	Levels					
	T <sub>1</sub>	T <sub>2</sub>	T <sub>3</sub>		T <sub>4</sub>	T <sub>5</sub>	F <sub>1</sub> (A)			F <sub>2</sub> (A)
W21	15	100	90	-	-	-	1.40	1.40	13	Medium size rounded defects plus almost interconnecting string of fade-out root defects.
W22	15	100	90	1	90	5	1.40	1.60	10	Reduced level of rounded defects. Root defect level reduced but still almost interconnecting.
W46	0	0	200	100	100	5	1.40	1.60	13	Large number of dispersed rounded defects plus root defects in fade-out region.
W47	0	0	200	60	90	5	1.40	1.60	16	Fine dispersion of rounded defects plus numerous small root defects.
W48	0	0	200	60	90	9	1.40	1.60	9	Long train of short root defects plus dispersion of rounded defects.
W49	0	0	200	60	90	9	1.40	1.60	9	Reduced level of root defects but some large rounded pores.
W52	0	20	200	40	90	9	1.40	1.60	24	Train of root defects, - smaller and less continuous. Some rounded pores. One 'shut-down' defect.
W53	5	0	200	20	90	9	1.40	1.60	9	Two very large round pores and fine dispersion of small rounded pores. Deep undercut caused by gun arc.

TABLE II. Effect of Beam Focus and Y Castellated Squarewave Oscillation Amplitude on Root Defect Formation

Specimen Number	Beam Current (mA)	Focus Coil Current (A)	Beam Oscillation						Root Defect Rating	Comments	
			X (along joint)			Y (across joint)					Combined Pattern
			mm	Hz	Pattern	mm	Hz	Pattern			
23	A	300	1.46	-	-	-	0	2000		(8)	) current
	B	300	1.46	-	-	-	0.5	2000		(6)	) excessive
	C	300	1.46	-	-	-	1.0	2000		(4)	)
	D	200	1.46	-	-	-	1.5	2000		4	20mm deep feathery defects
	E	200	1.46	-	-	-	2.0	2000		5	20mm deep feathery defects
	F	200	1.46	-	-	-	2.5	2000		4	20mm deep feathery defects
24	A	200	1.48	-	-	-	0	2000		9	No apparent defects
	B	200	1.48	-	-	-	0.5	2000		8.5	Faint 15mm deep defects
	C	200	1.48	-	-	-	1.0	2000		7	15mm deep defects
	D	200	1.48	-	-	-	1.5	2000		6	} intermittent 15 - 20mm defects
	E	200	1.48	-	-	-	2.0	2000		6	
	F	200	1.48	-	-	-	2.5	2000		6.5	
25	A	200	1.50	-	-	-	0	2000		8.5	Very narrow faint defects
	B	200	1.50	-	-	-	0.5	2000		8	15mm deep feathery defects
	C	200	1.50	-	-	-	1.0	2000		7	20mm deep feathery defects
	D	200	1.50	-	-	-	1.5	2000		7	20mm deep feathery defects
	E	200	1.50	-	-	-	2.0	2000		8	20mm deep feathery defects
	F	200	1.50	-	-	-	2.5	2000		8	Intermittent defects

TABLE III. Effect of Y Oscillation for Two Amplitudes

Specimen Number	Beam Current (mA)	Focus Coil Current (A)	Beam Oscillation						Root Defect Rating	Comments	
			X (along joint)			Y (across joint)					Combined Pattern
			mm	Hz	Pattern	mm	Hz	Pattern			
26	A	200	1.500	-	-	-	4	14		3	Large cluster defects
	B	200	1.500	-	-	-	4	140		7½	7mm almost cont. defects.
	C	200	1.500	-	-	-	4	1400		6	10mm deep defect
	D	200	1.500	-	-	-	4	2800		7	12mm deep defect
27	A	200	1.500	-	-	-	2	14		7	Faint deep defects
	B	200	1.500	-	-	-	2	140		8	10mm deep defects
	C	200	1.500	-	-	-	2	1400		7	12mm deep defects
	D	200	1.500	-	-	-	2	2800		6	15mm deep defects

TABLE IV. Effect of Focus for 4mm Y Castellated Oscillation

Specimen Number	Beam Current (mA)	Focus Coil Current (A)	Beam Oscillation					Root Defect Rating	Comments		
			X (along joint)			Y (across joint)				Combined Pattern	
			mm	Hz	Pattern	mm	Hz				Pattern
28	A	200	1.400	-	-	-	4	140		5	12-15mm deep defects
	B	200	1.450	-	-	-	4	140		6	7mm deep defects
	C	200	1.500	-	-	-	4	140		6	5.5mm deep defects
	D	200	1.550	-	-	-	4	140		5	6mm deep defects

TABLE V. Effect of Triangular Oscillation Pattern

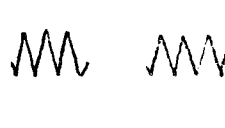
Specimen Number	Beam Current (mA)	Focus Coil Current (A)	Beam Oscillation					Root Defect Rating	Comments		
			X (along Joint)			Y (across joint)				Combined Pattern	
			mm	Hz	Pattern	mm	Hz				Pattern
29	A	200	1.500	-	-	-	2	50		4	35mm deep defects
	B	200	1.500	-	-	-	2	70		7	Faint 10-15mm deep defects
	C	200	1.500	-	-	-	2	140		6	Faint 15-20mm deep defects
	D	200	1.500	-	-	-	2	210		5	20-30mm deep defects

TABLE VI. Effect of X-Y Raster Parameters

Specimen Number	Beam Current (mA)	Focus Coil Current (A)	Beam Oscillation					Root Defect Rating	Comments		
			X (along joint)			Y (across joint)				Combined Pattern	
			mm	Hz	Pattern	mm	Hz				Pattern
30	A	200	2	5000	} 	2	140	} 	} 	8.5	Intermittent faint defects.
	B	200	3	5000		2	140			5	Narrow 10-25mm deep defects
	C	200	4	5000		2	140			3	2-3mm wide full depth defects
	D	200	5	5000		2	140			1	3-4mm wide full depth defects

TABLE VII. Effect of Figure of Eight Lissajous Pattern Parameters

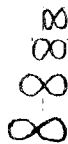
Specimen Number	Beam Current (mA)	Focus Coil Current (A)	Beam Oscillation					Root Defect Rating	Comments		
			X (along joint)			Y (across joint)				Combined Pattern	
			mm	Hz	Pattern	mm	Hz				Pattern
31	A	200	2	2000	} 	2	4000	} 	} 	7.5	Faint 5-10mm deep defects
	B	200	3	2000		2	4000			7	Faint 5-10mm deep defects
	C	200	4	2000		2	4000			6	10-25mm deep defects plus root defects
	D	200	5	2000		2	4000			5	10-30mm deep defects plus root defects
32	A	200	0	2000	} 	0	4000	} 	} 	8	Faint 10-15mm deep defects
	B	200	0.5	2000		0.5	4000			8	Faint 10-15mm deep defects
	C	200	1.0	2000		1.0	4000			7.5	Faint 10-15mm deep defects
	D	200	1.5	2000		1.5	4000			7	Faint 10-15mm deep defects

TABLE VIII. Effect of High Frequency Concentric Circles Deflection Pattern

Specimen Number	Beam Current (mA)	Focus Coil Current (A)	Beam Oscillation						Root Defect Rating	Comments		
			X (along joint)			Y (across joint)					Combined Pattern	
			mm	Hz	Pattern	mm	Hz	Pattern				
37	B	200	1.340	1.3	236,000	-	1.3	236,000	-	⊙	7	10-12mm deep defects
	C	200	1.340	1.8	236,000	-	1.8	236,000	-		6.5	10-15mm deep defects
	D	200	1.340	2.0	236,000	-	2.0	236,000	-		6.5	10-15mm deep defects

TABLE IX. Effect of Welding Speed

Specimen Number	Beam Current (mA)	Welding Speed (mm/min)	Focus Coil Current (A)	Penetration Depth	Root Defect Rating	Comments
38	A	500	1.400	60	6	Cont. train 10-12mm root defects
	B	500	1.400	85	5.5	Cont. train 10-15mm root defects
39	A	500	1.400	100	6.5	Large root pores
	B	500	1.400	85-90	6	Cont. train 10-15mm root defects
	C	500	1.400	70	6	Cont. train 10-15mm root defects
	D	500	1.400	60	6	Cont. train 10-15mm root defects

TABLE X. Welding Conditions Used For First Simulated Lid Weld

Specimen Number	Accel. Volt. kV	Surface Tra-verse speed mm/min	Working Distance mm	Beam Current							Slope Shape No.	Focus			
				Tack Weld mA	Main Weld mA	Slope Shape No.	Time Periods (secs)					Time Periods		Levels A	
							T <sub>1</sub>	T <sub>2</sub>	T <sub>3</sub>	Overlap		T <sub>4</sub>	T <sub>5</sub>	F1	F2
W55	143	120	150	75	500	5	5	997	200	60	9	40	90	1.400	1.600

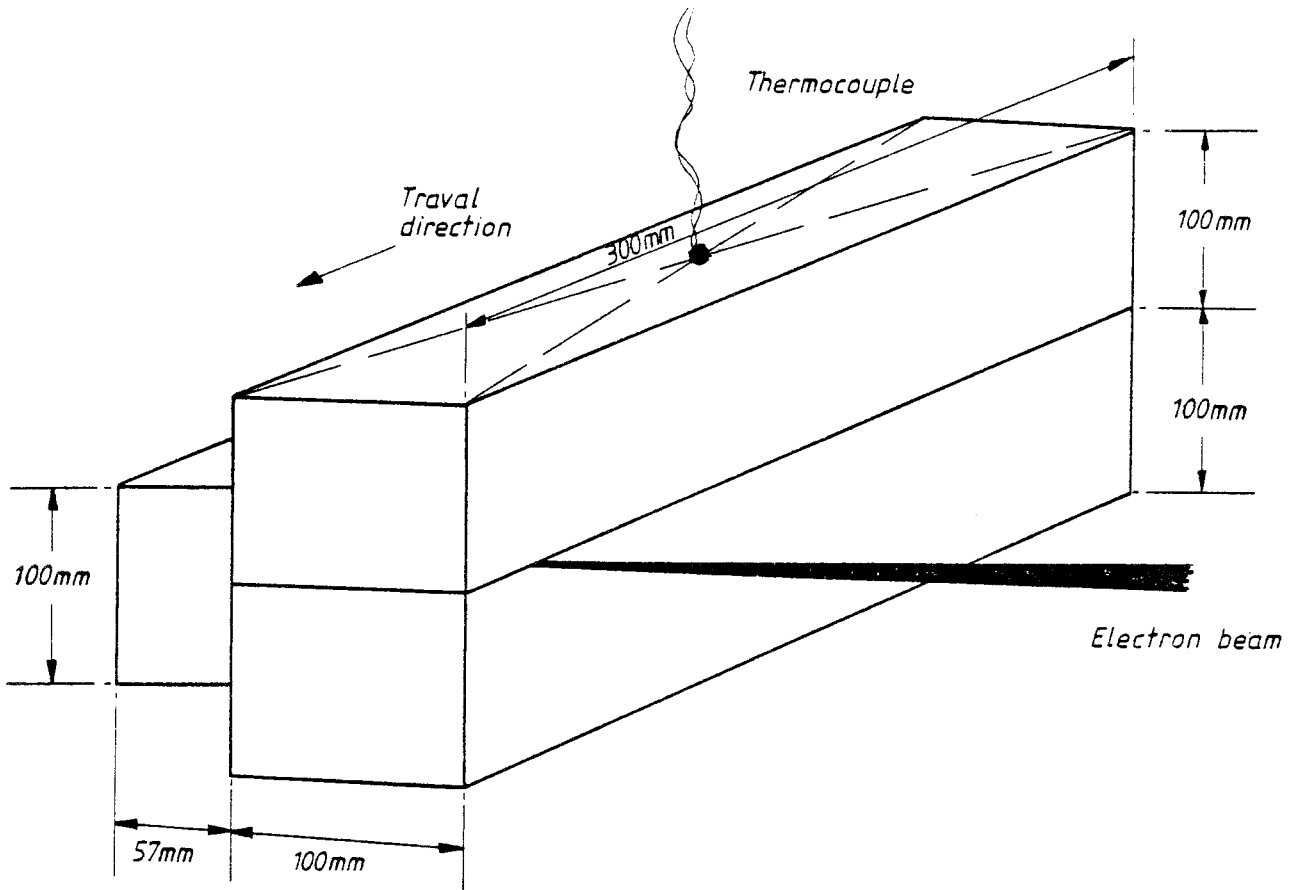


Fig. 1. Standard copper block assembly used for weld overlap and beam fade-out trials.

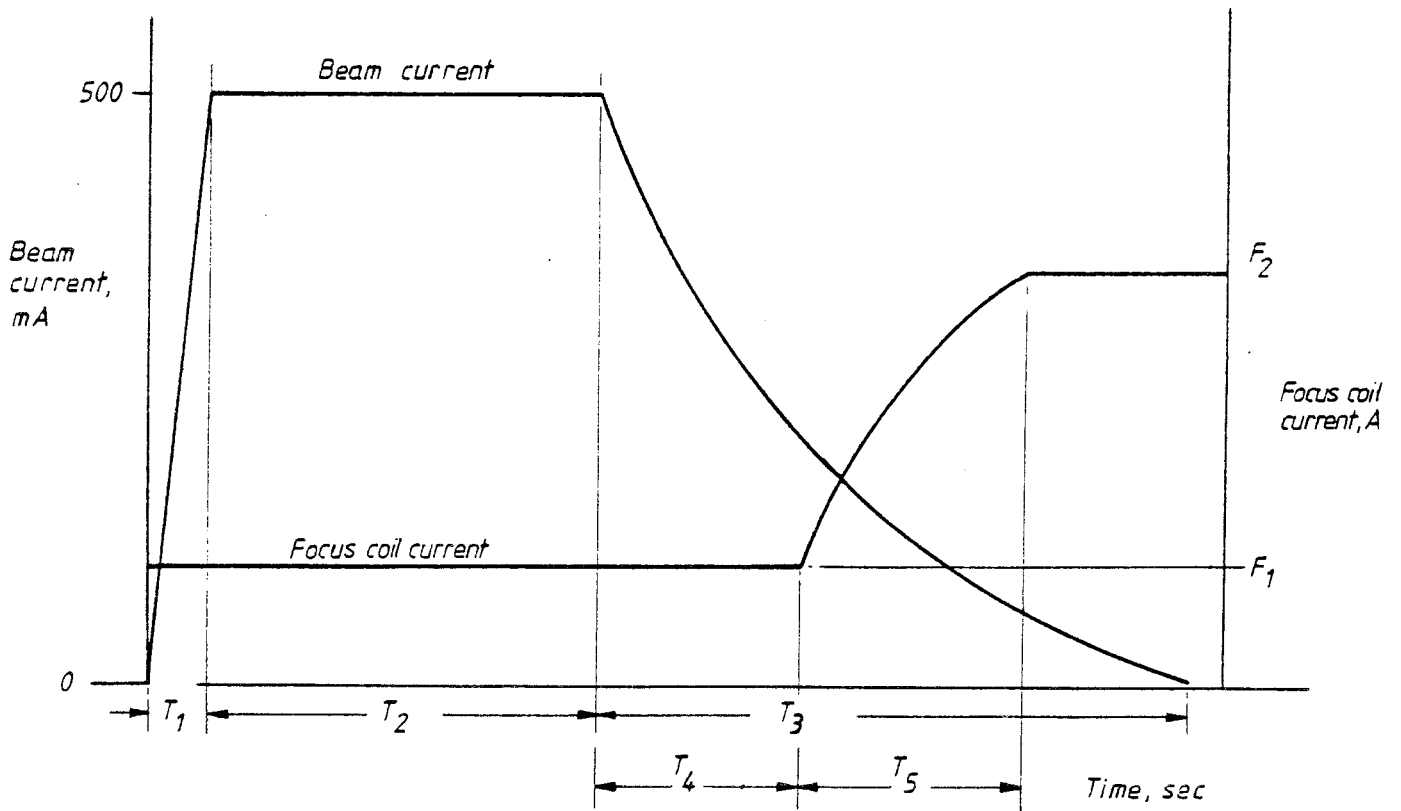


Fig. 2. Time-parameter level relationship between beam current and focus coil current for weld overlap and beam fade-out trials.

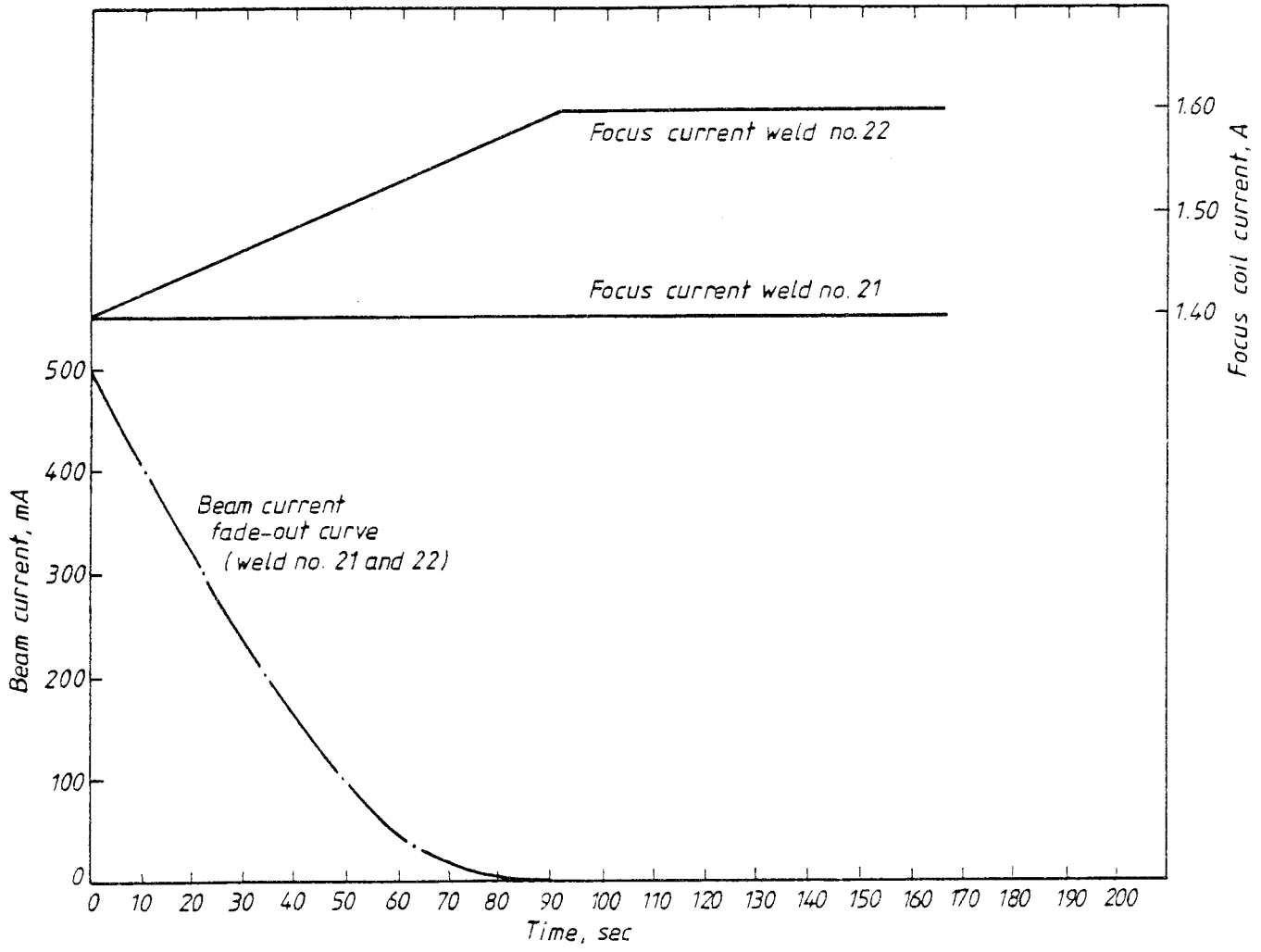
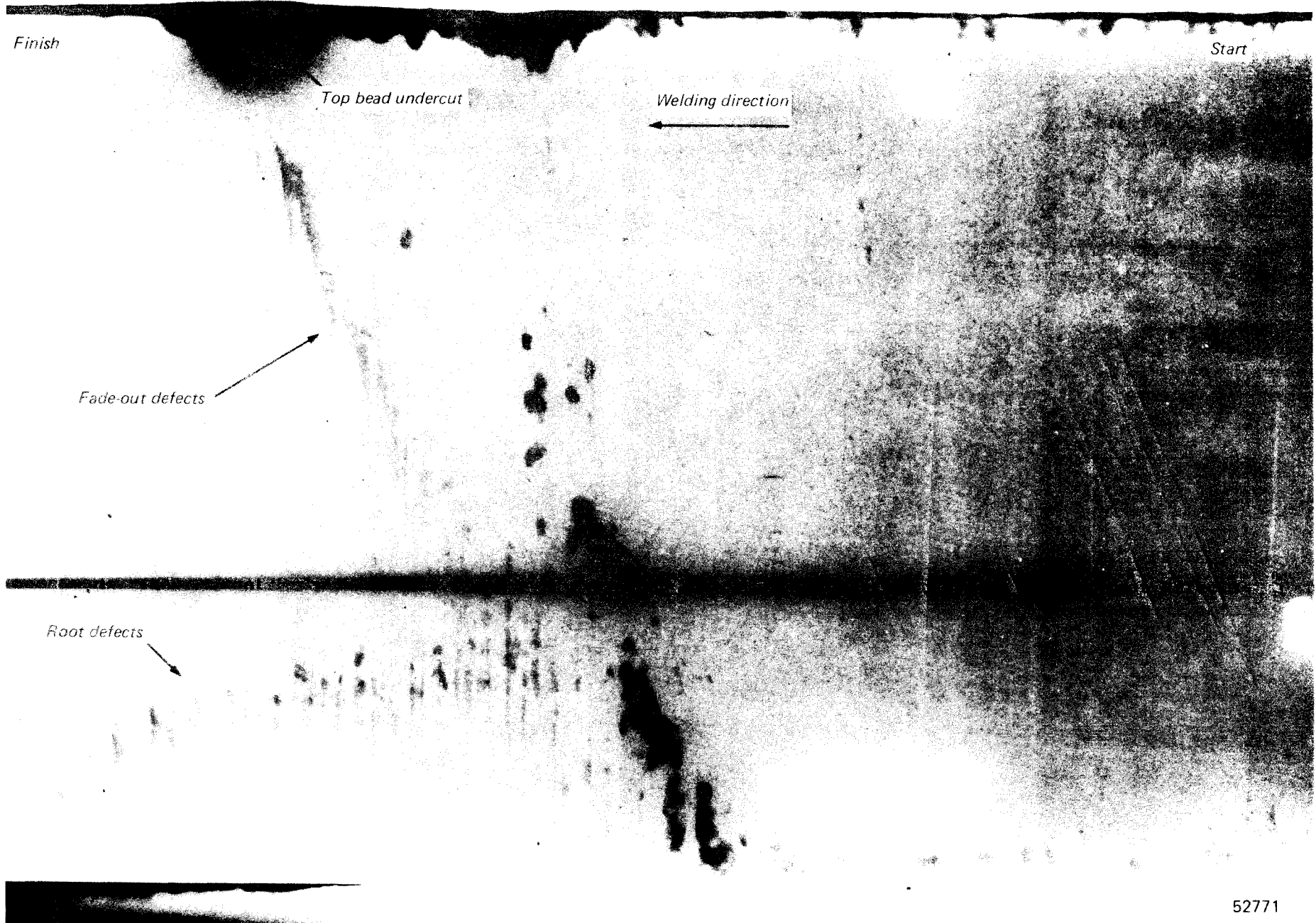


Fig.3. Beam current and focus ramp curves for weld numbers 21 and 22.



52771

Fig.4. Radiograph of weld number 21 showing train of root defects in beam fade out-region and other medium sized defects.

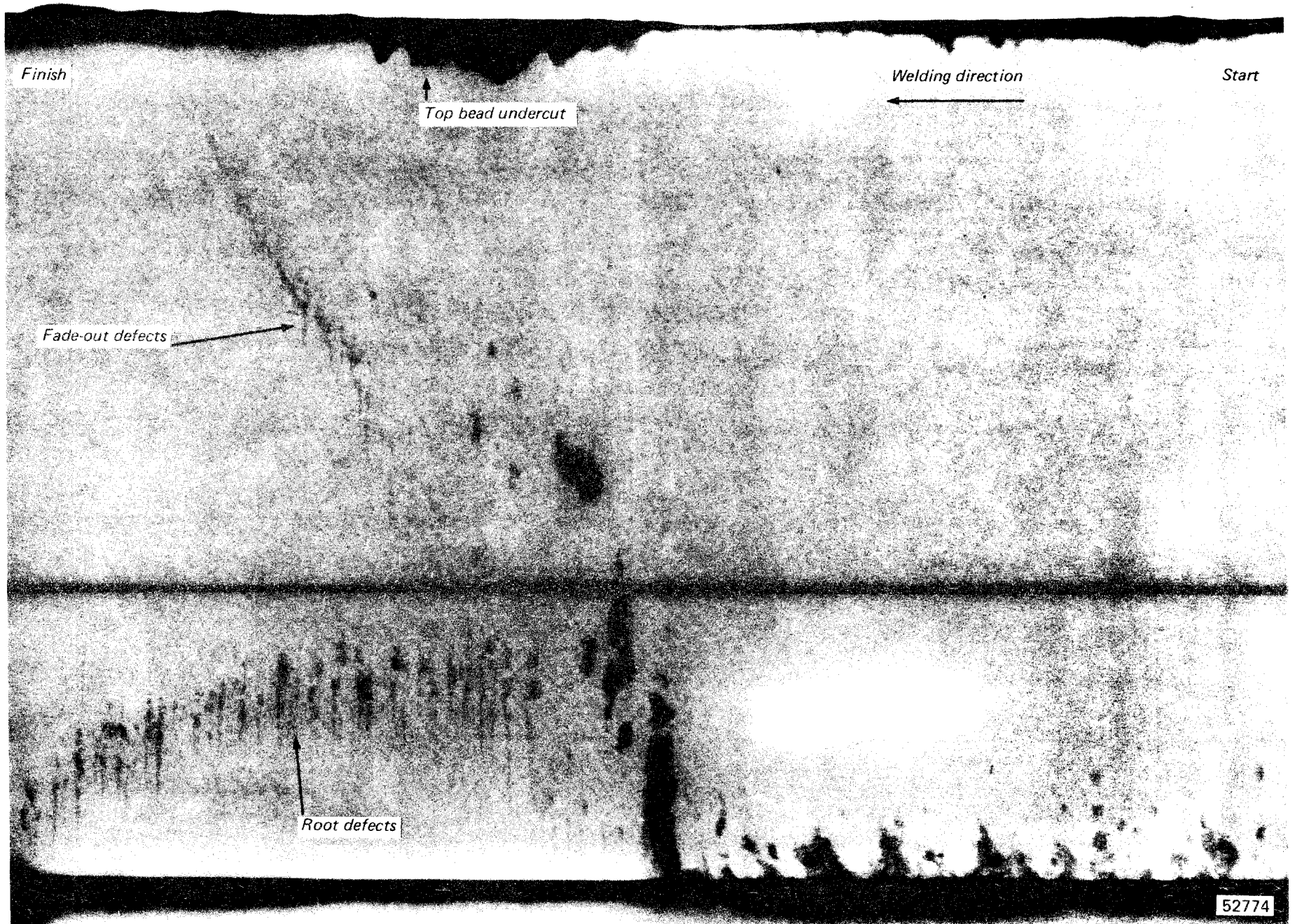


Fig.5. Radiograph of weld number 22 showing reduced defect and undercut level compared with weld number 21, Fig.4.

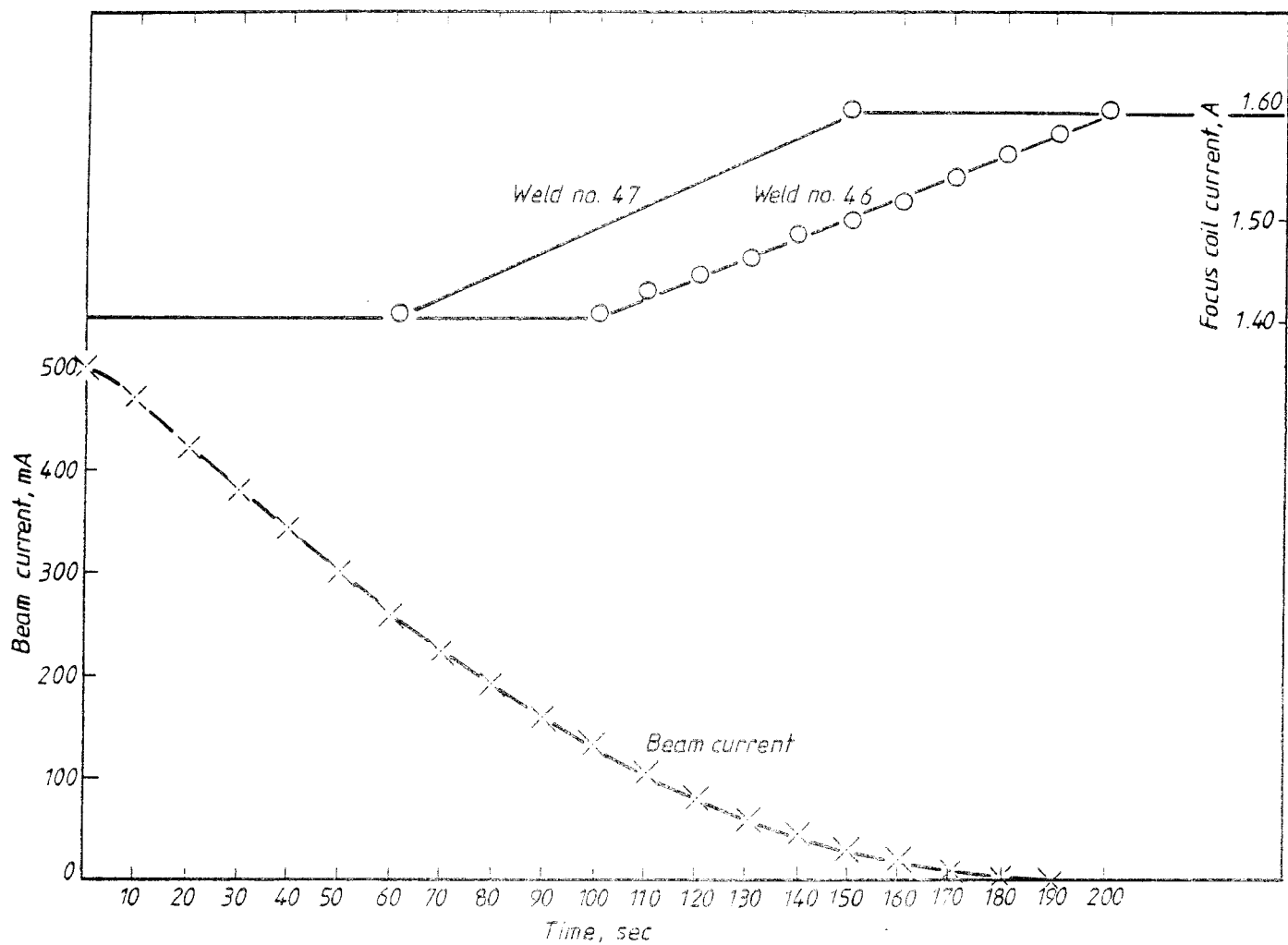
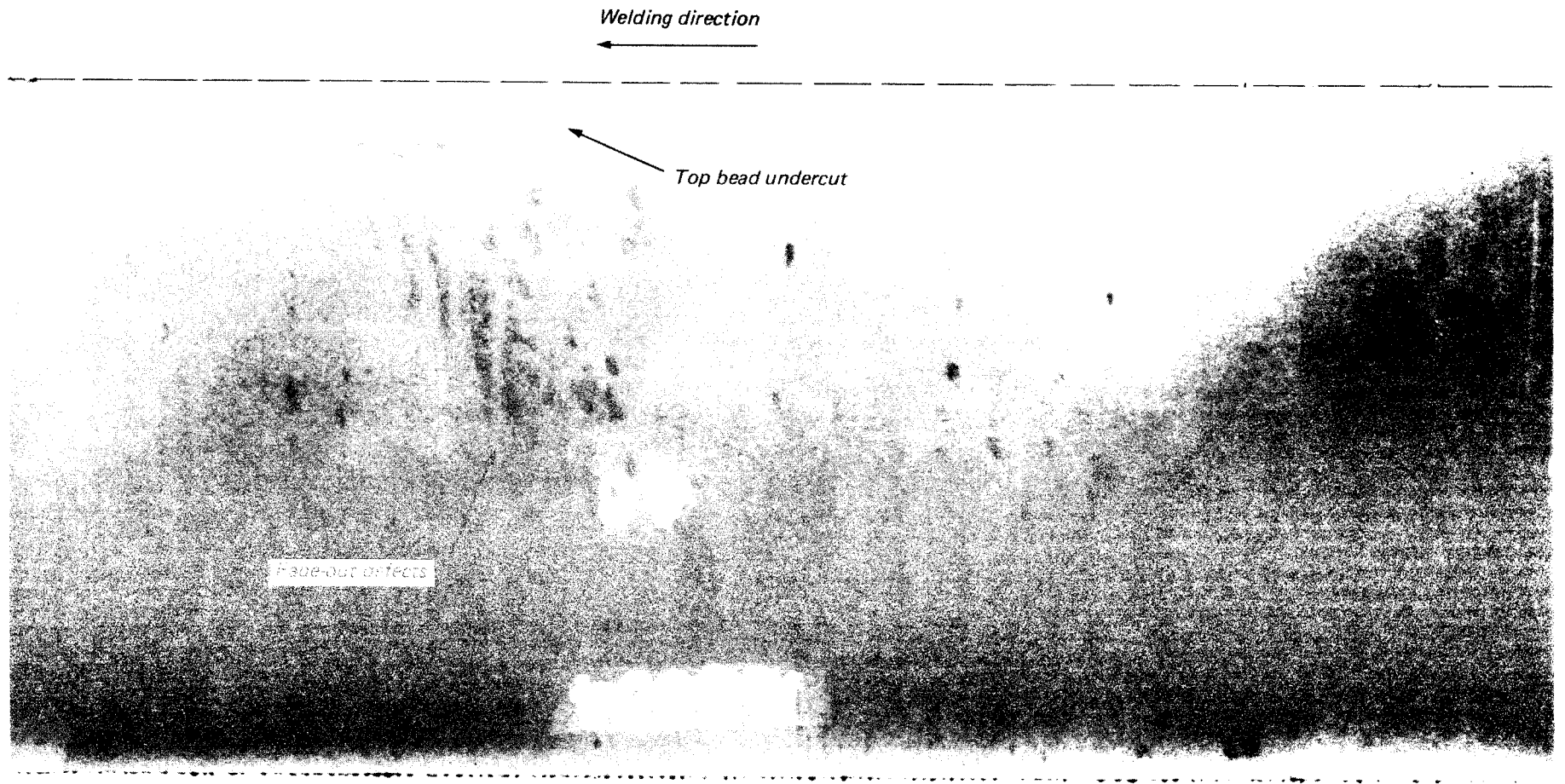
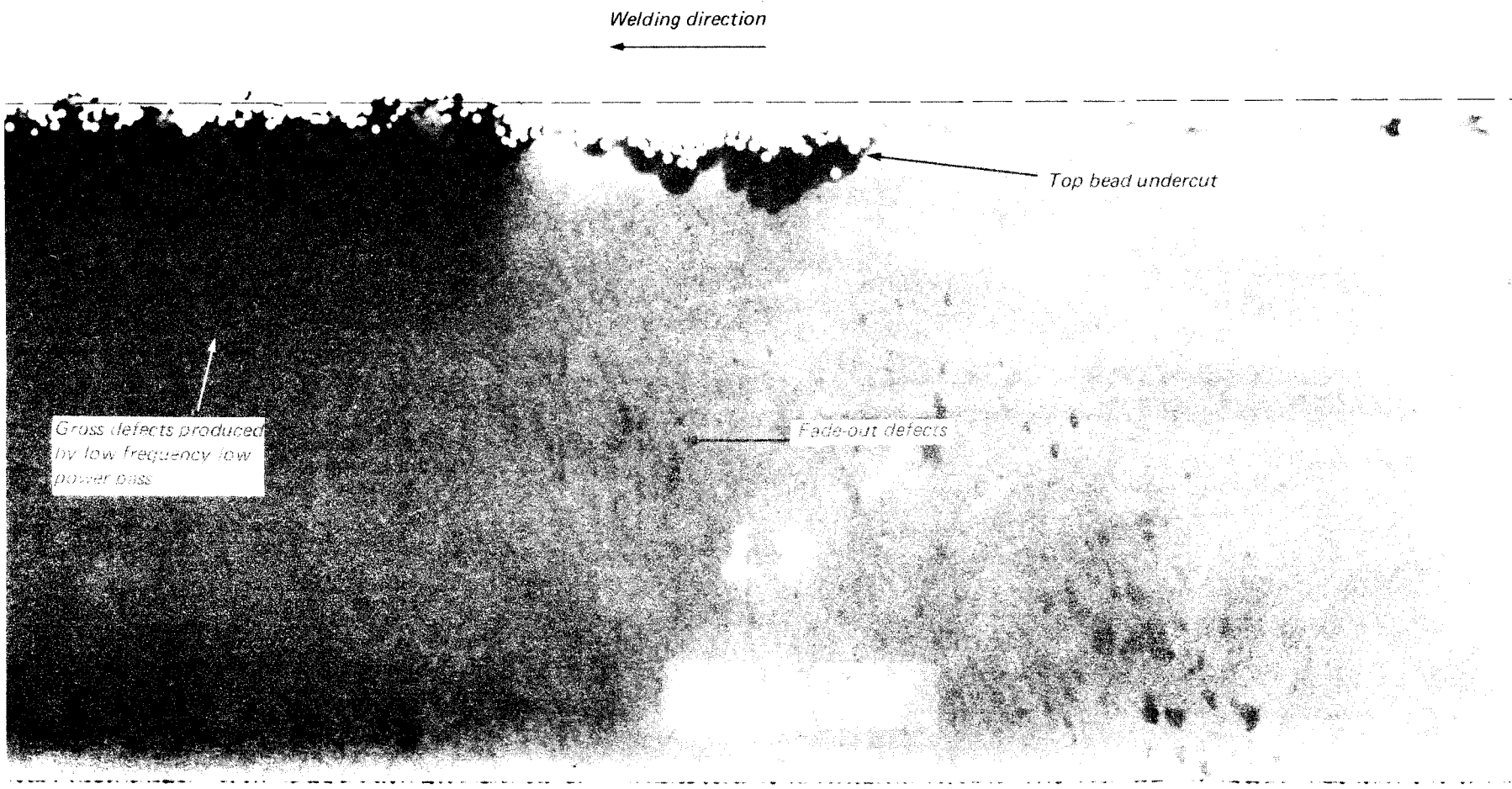


Fig.6. Beam current and focus ramp curves for weld numbers 46 and 47.



52773

*Fig.7. Radiograph of weld number 46, note increased defect and undercut level of Fig.4 and 5.*



52772

*Fig.8. Radiograph of weld number 47 showing improved fade-out defect level compared with Fig.7.*

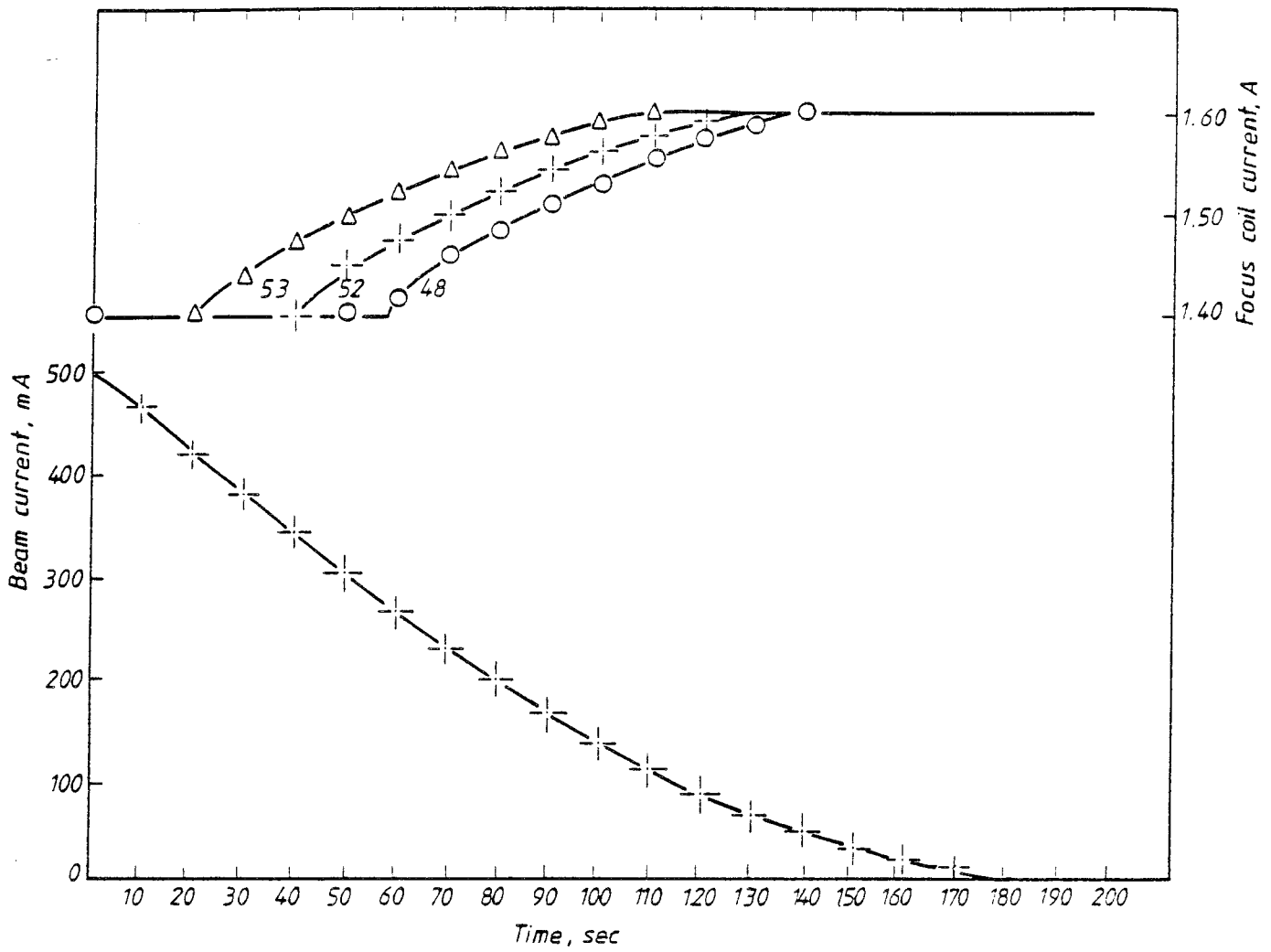
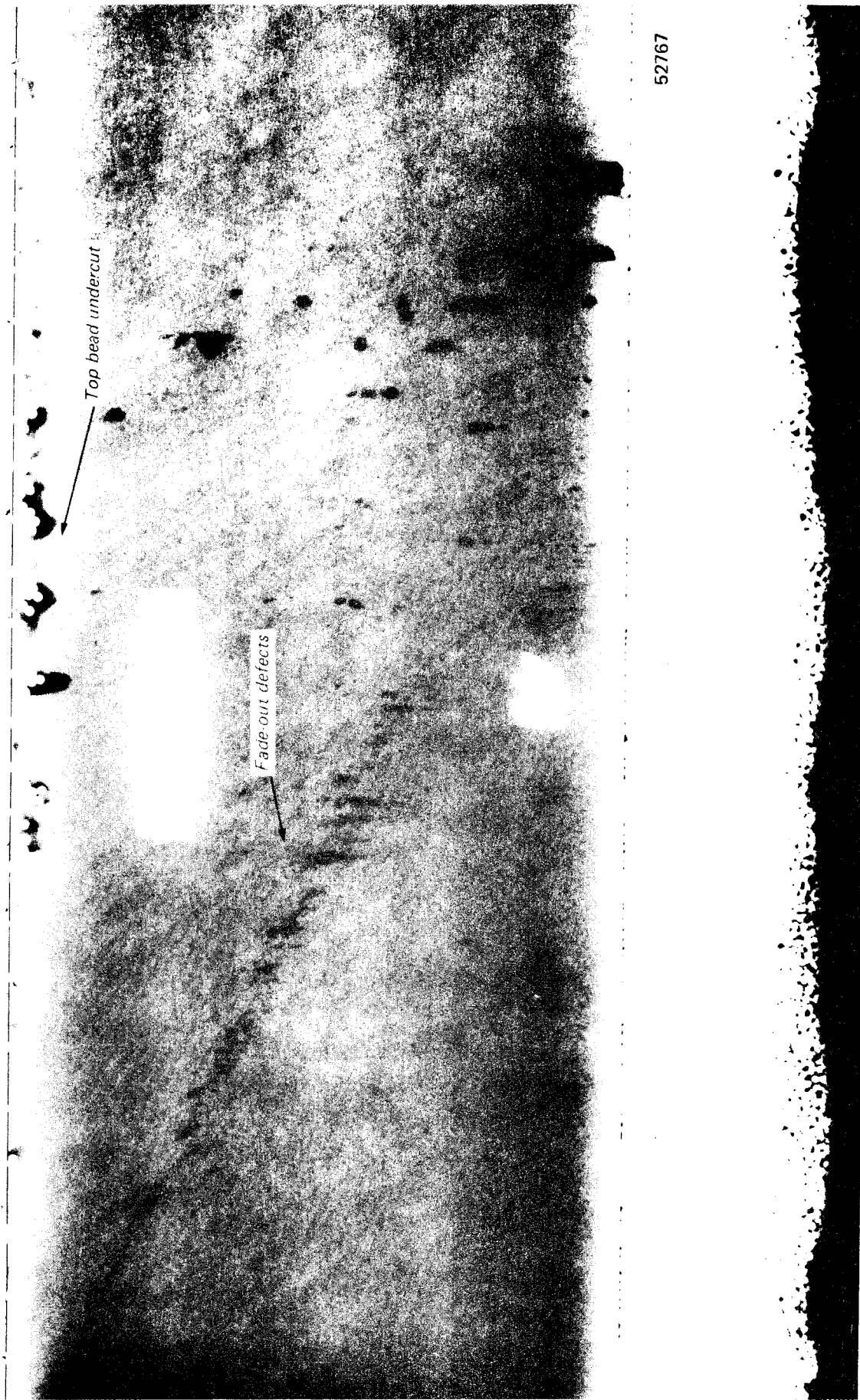


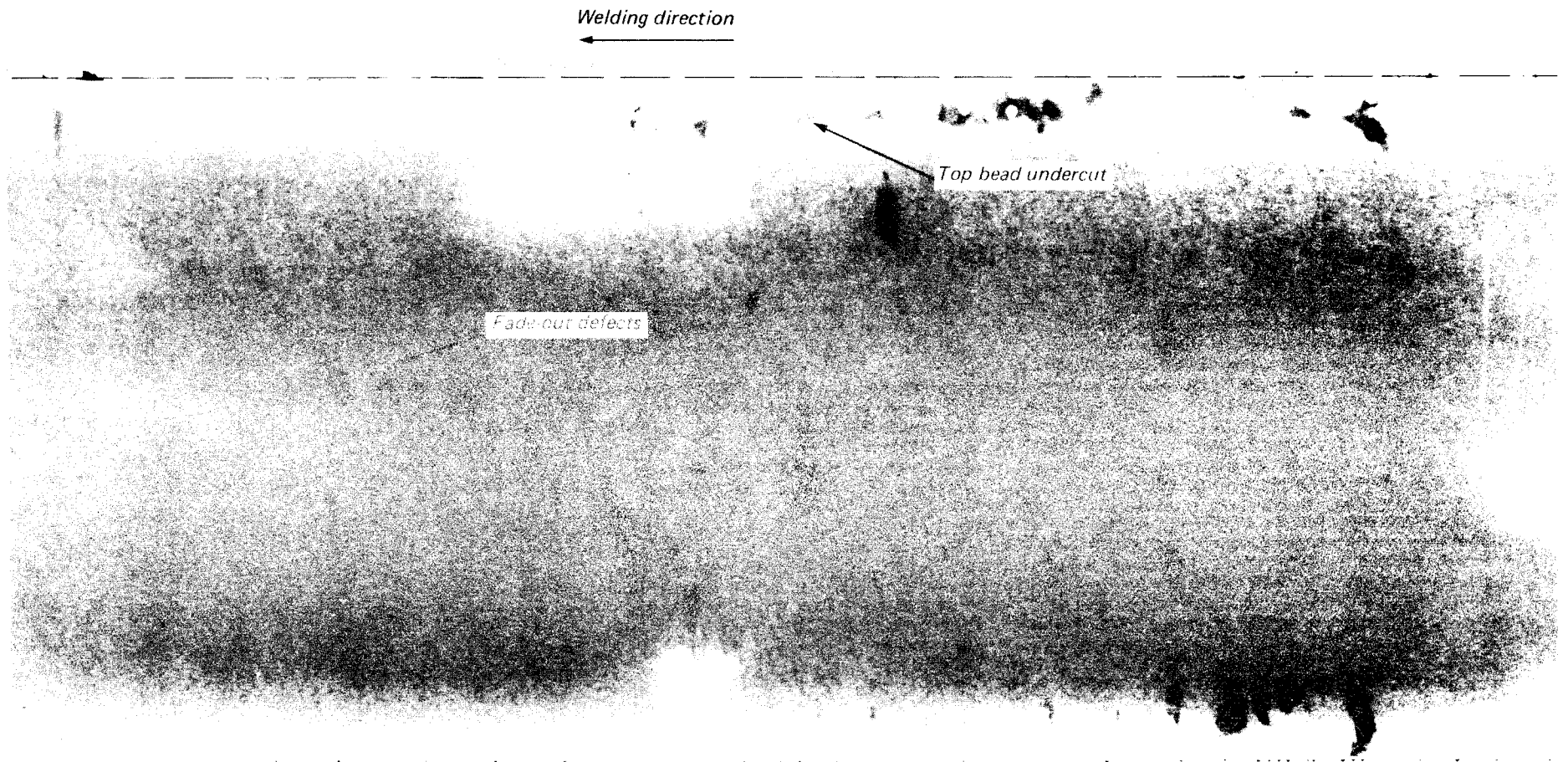
Fig.9. Beam current and focus ramp curves for weld numbers 48, 52 and 53.

Welding direction



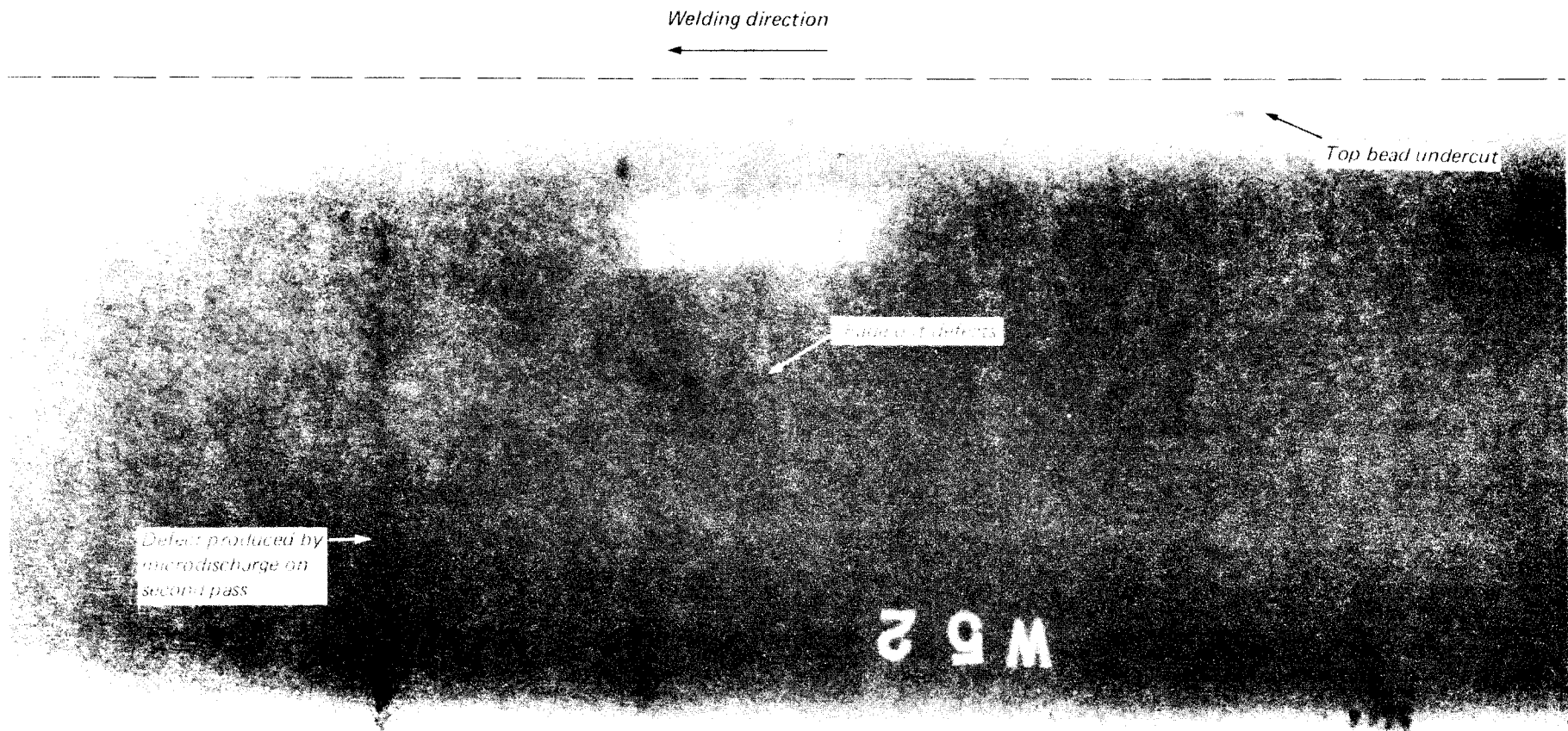
52767

Fig. 10. Radiograph of weld number 48, showing reduced top bead undercutting but almost continuous train of fade-out defects.



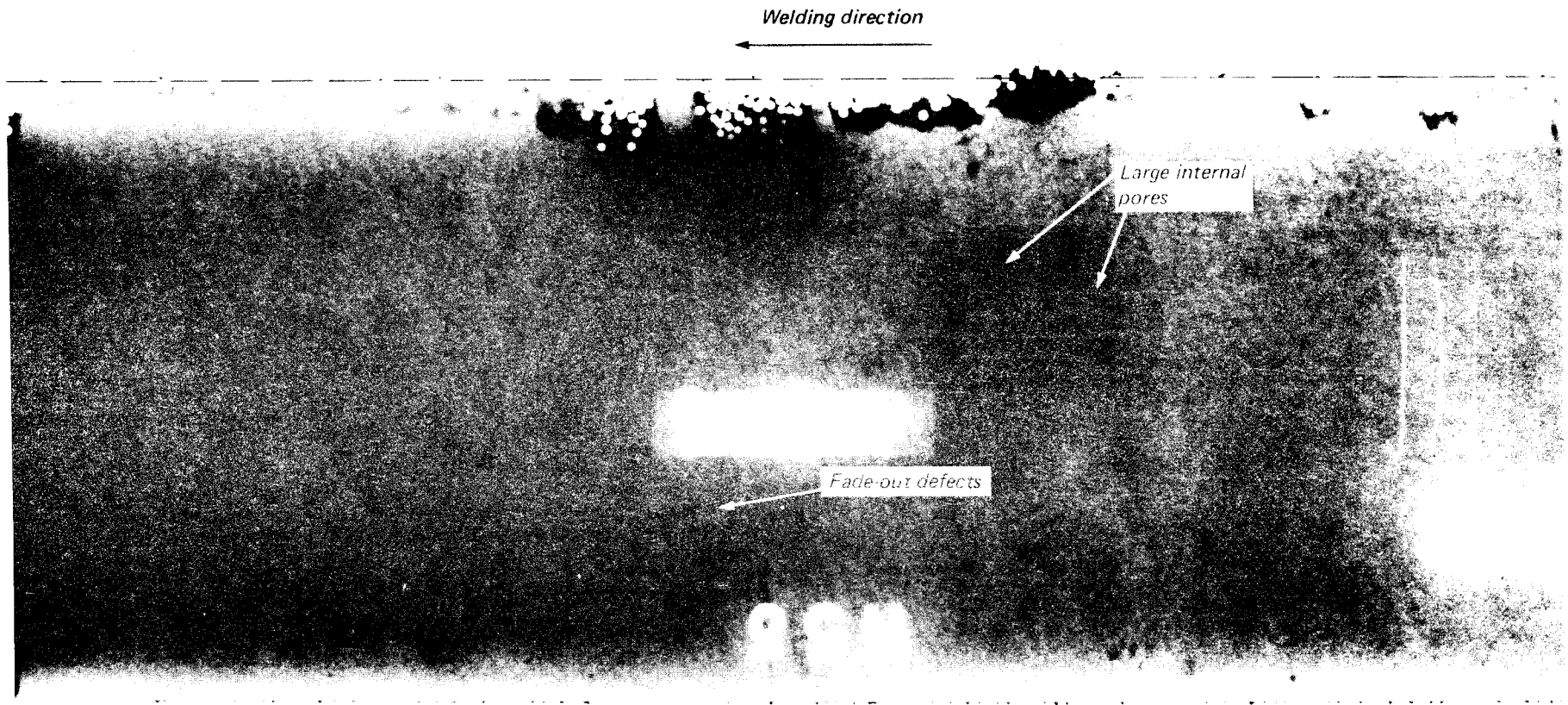
52769

*Fig. 11. Radiograph of weld number 49 made with low beam current ripple supply.*



52768

*Fig.12. Radiograph of weld number 52 showing improved top bead undercut and fade-out defect level.*



52770

*Fig. 13. Radiograph of weld number 53. Note this condition appeared generally to improve the fade-out root defect level but resulted in deep undercut and large internal defects.*

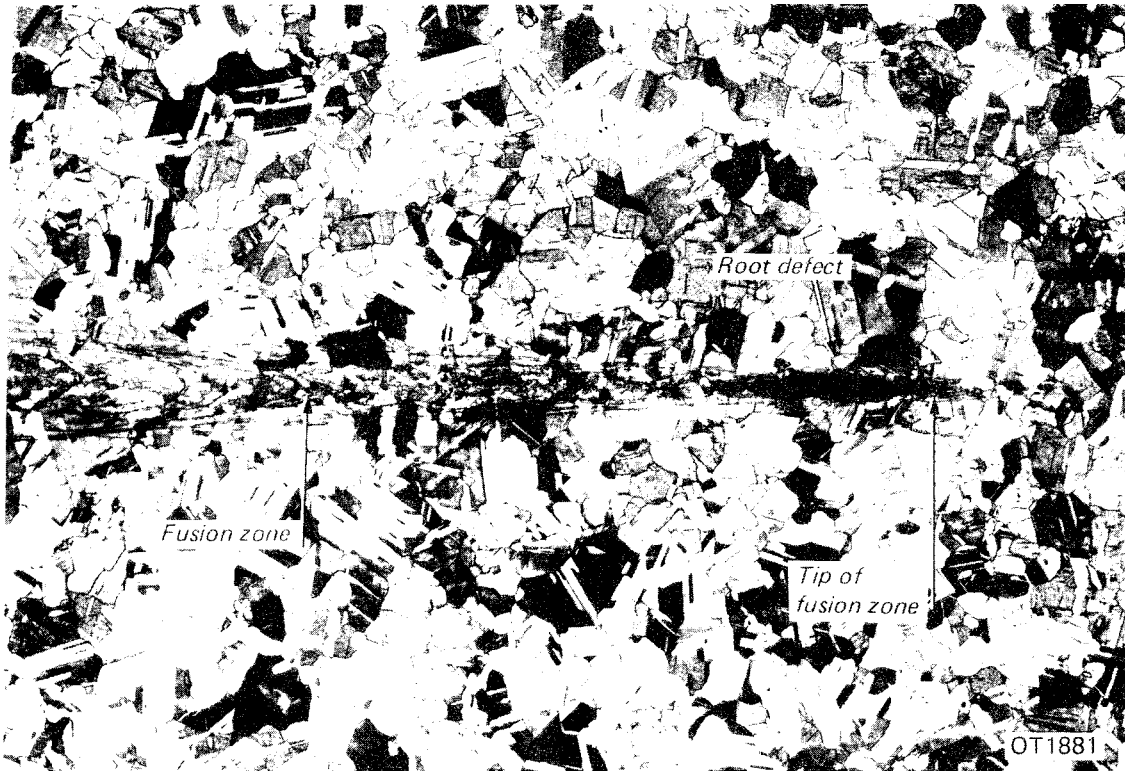


Fig.14. Macrograph of specimen number 24A showing narrow penetration finger tip and root defect, x7.

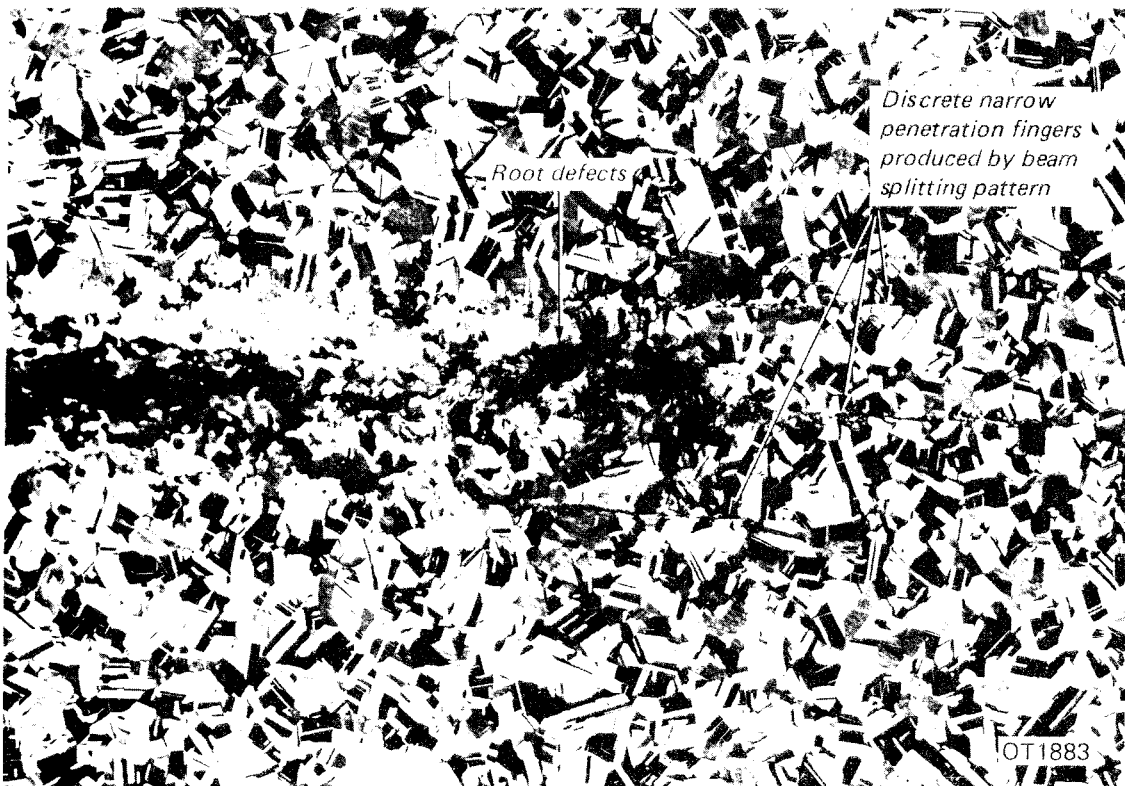
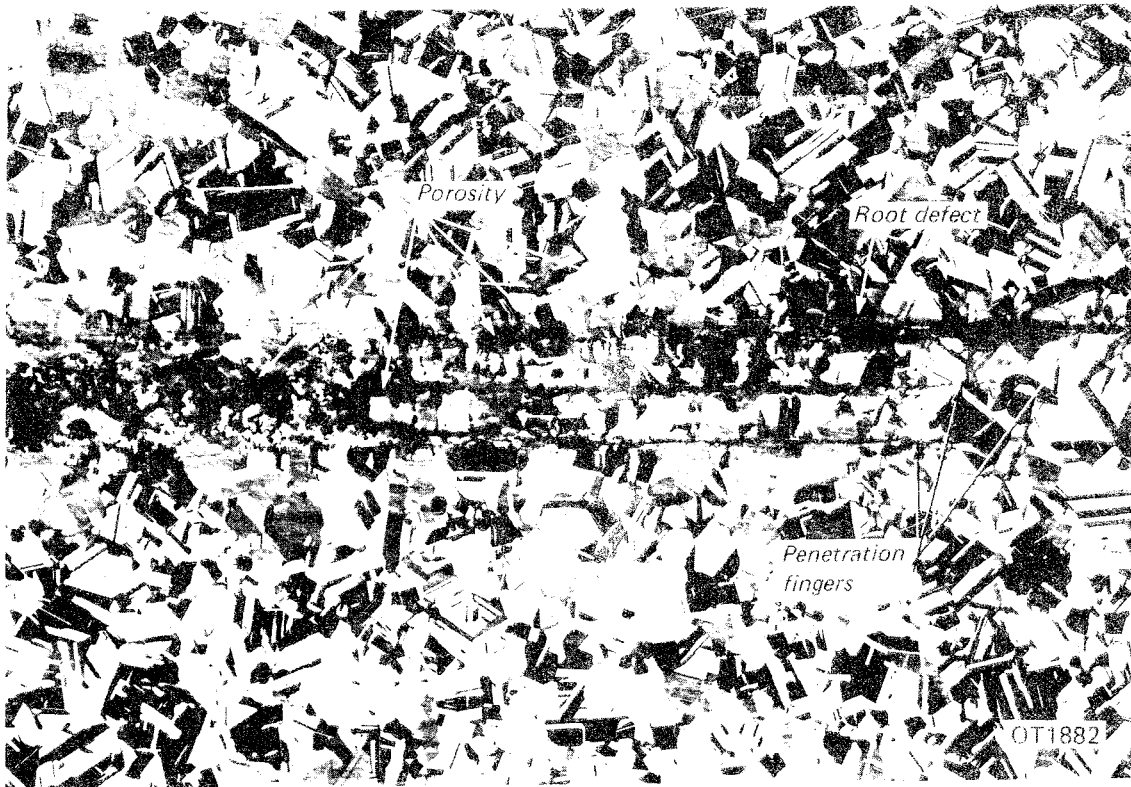


Fig.15. Macrograph of specimen number 26B showing generally rounded fusion zone tip produced by castellated oscillation pattern, x7.



*Fig. 16. Macrograph of specimen number 27A showing three distinct penetration fingers and porosity, x7.*

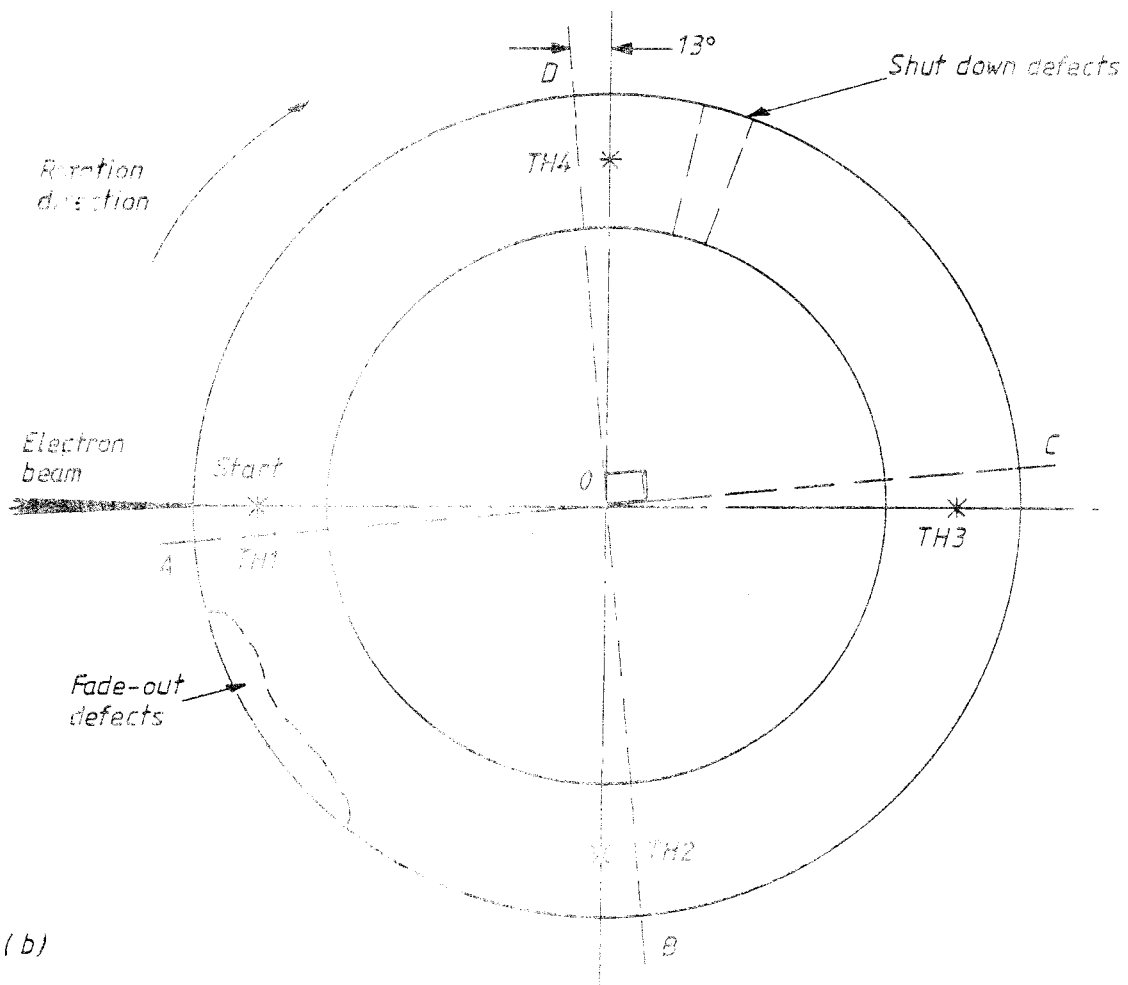
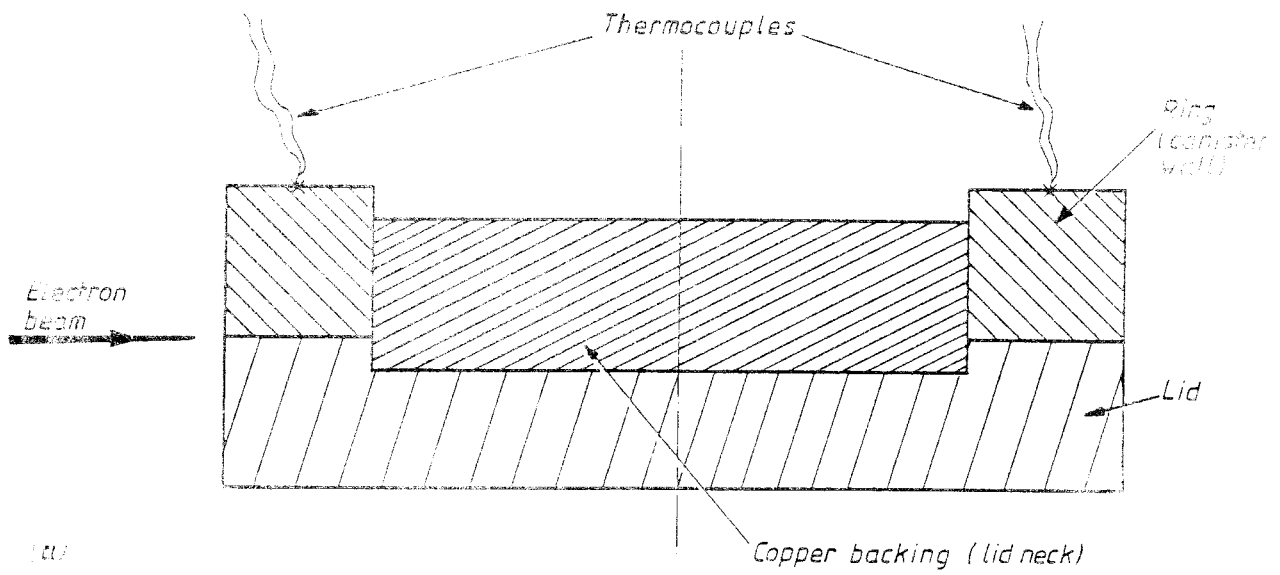


Fig. 12. Quarantined copper lid assembly:  
 (a) elevation (b) plan (first angle projection)



52481

*Fig. 18. General view of simulated lid assembly as-welded.*

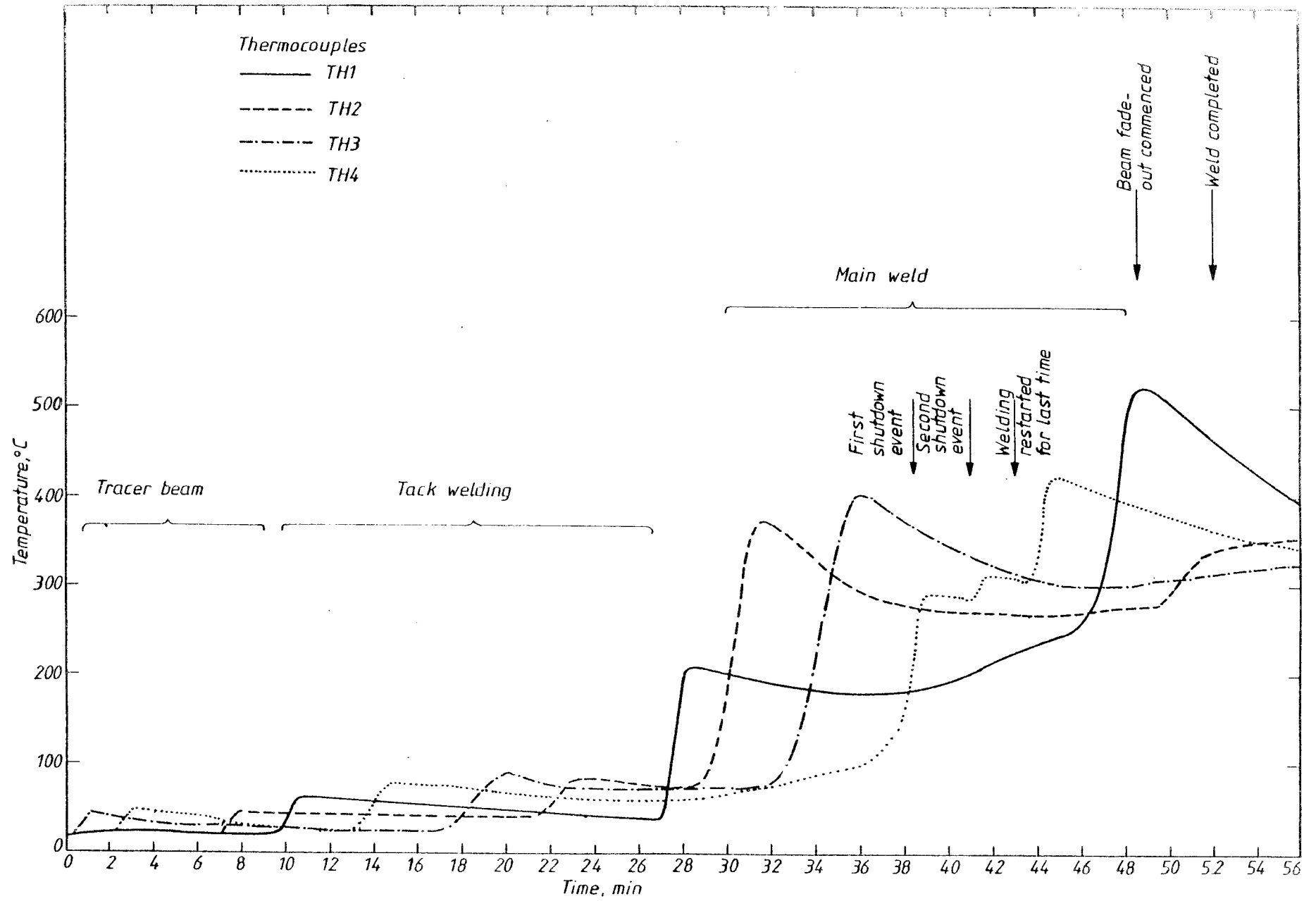


Fig. 19. Thermocouple measurements.

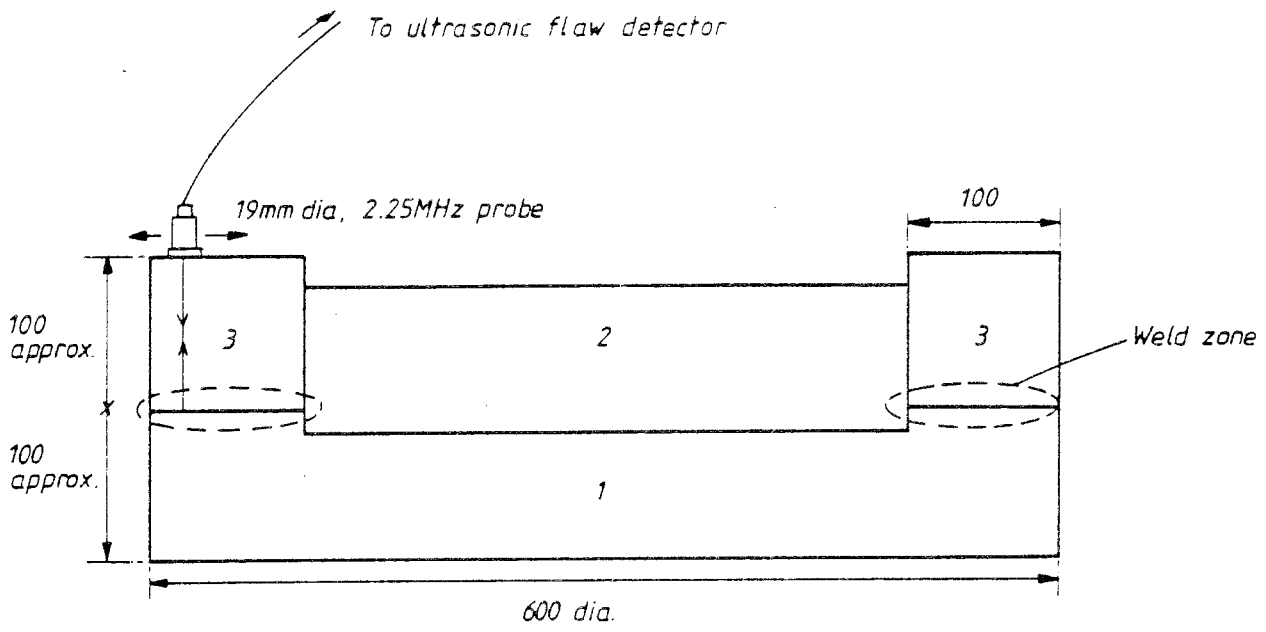


Fig.20. Contact scanning. Cross-sectional view of specimen. (Dimensions in mm.)



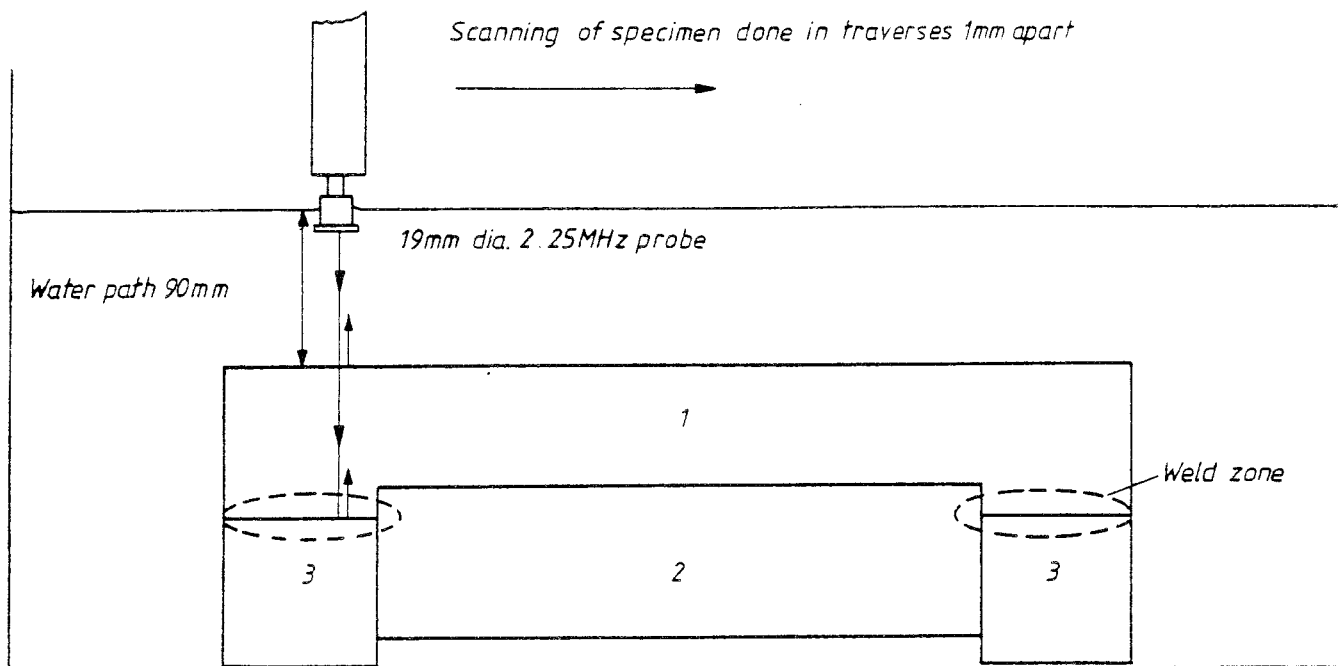


Fig.22. Immersion scanning.

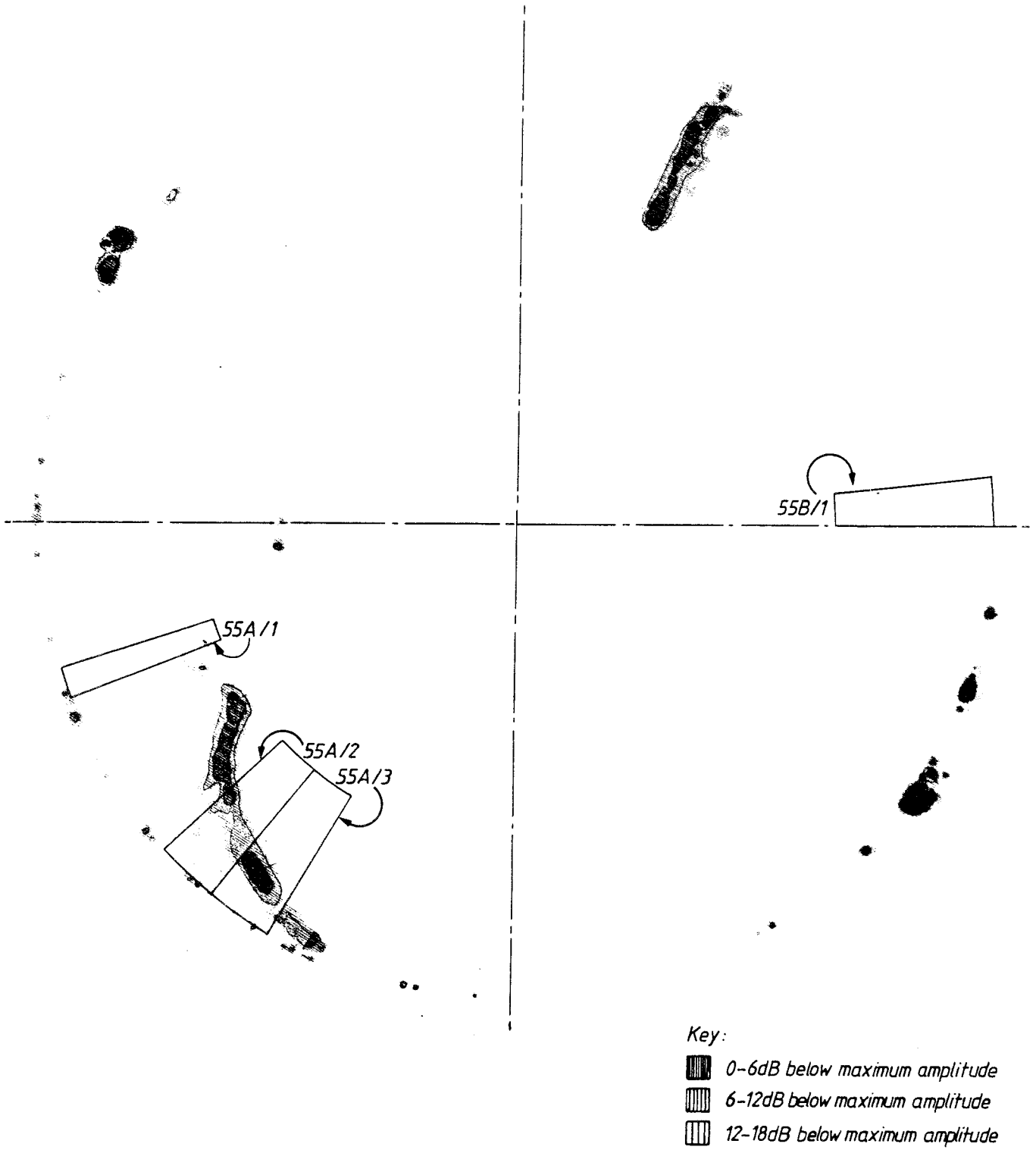


Fig.23. Immersion ultrasonic C scan. Maximum signal amplitude at arrowed point.

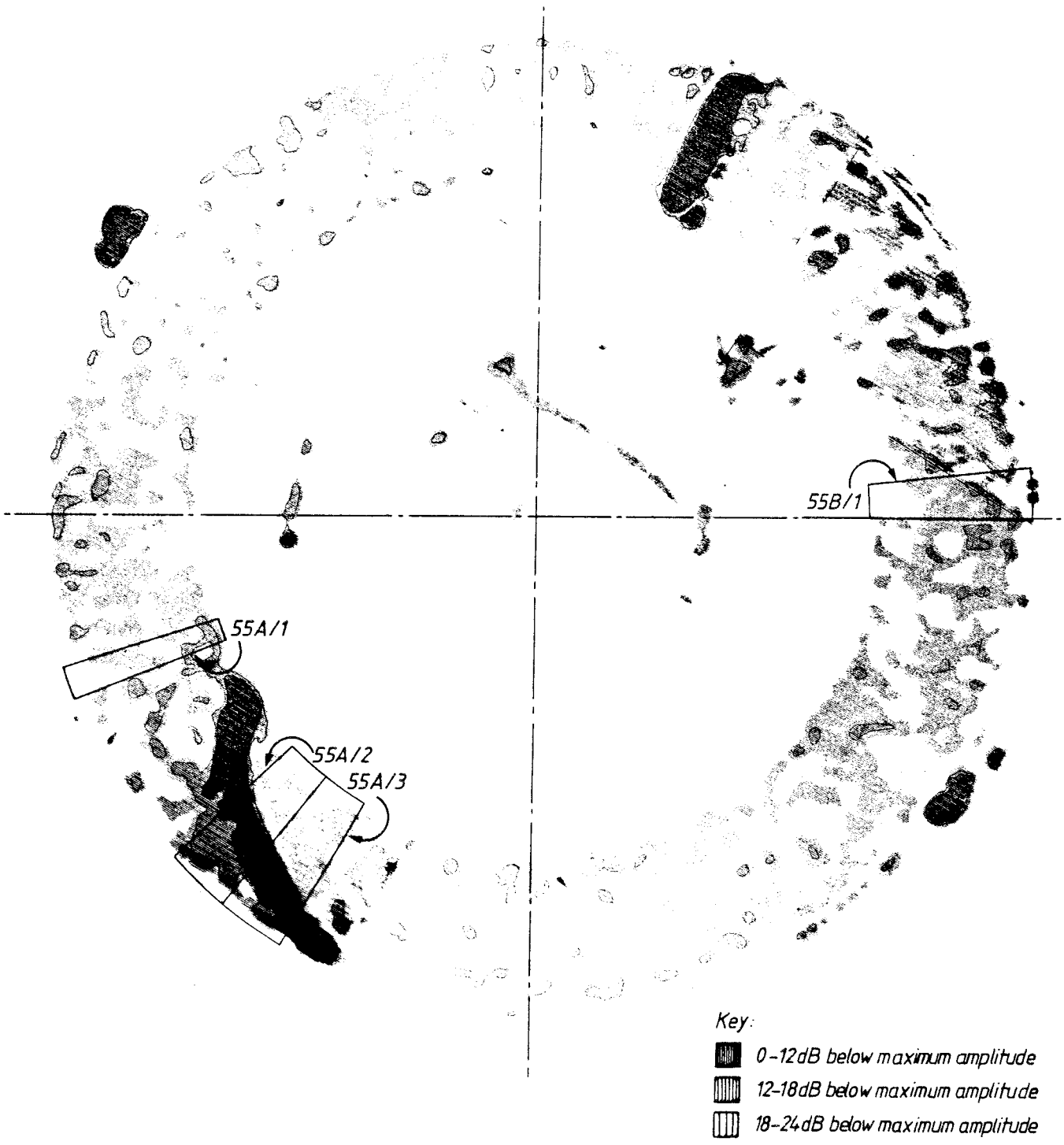


Fig.24. Immersion ultrasonic C-scan. Scan sensitivity increased by 6dB.

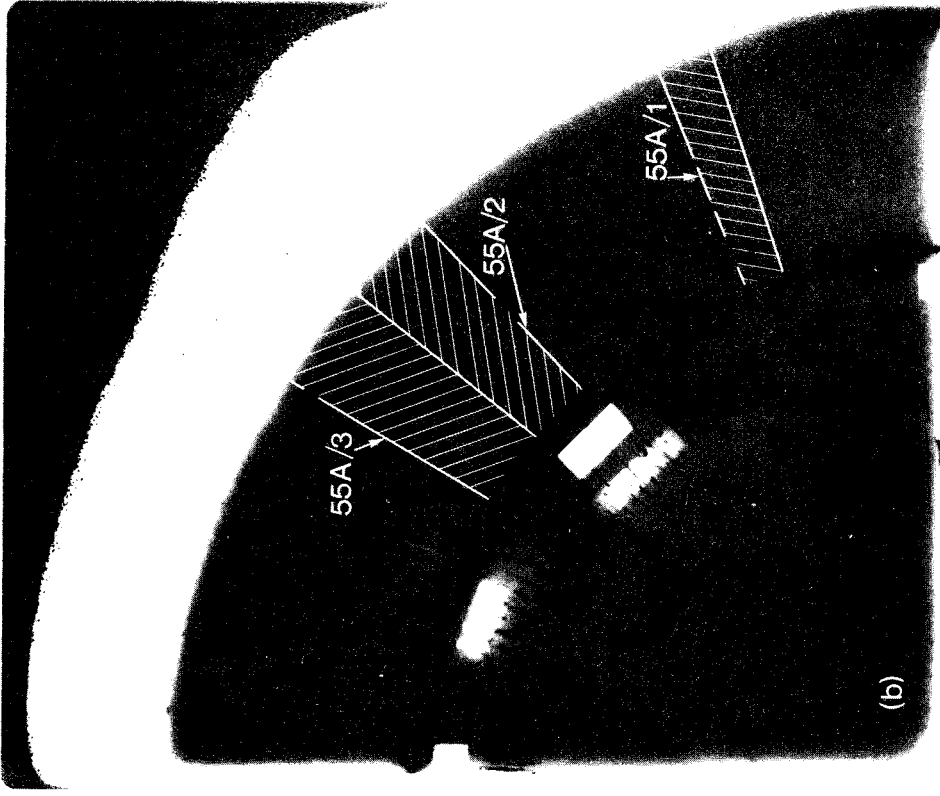
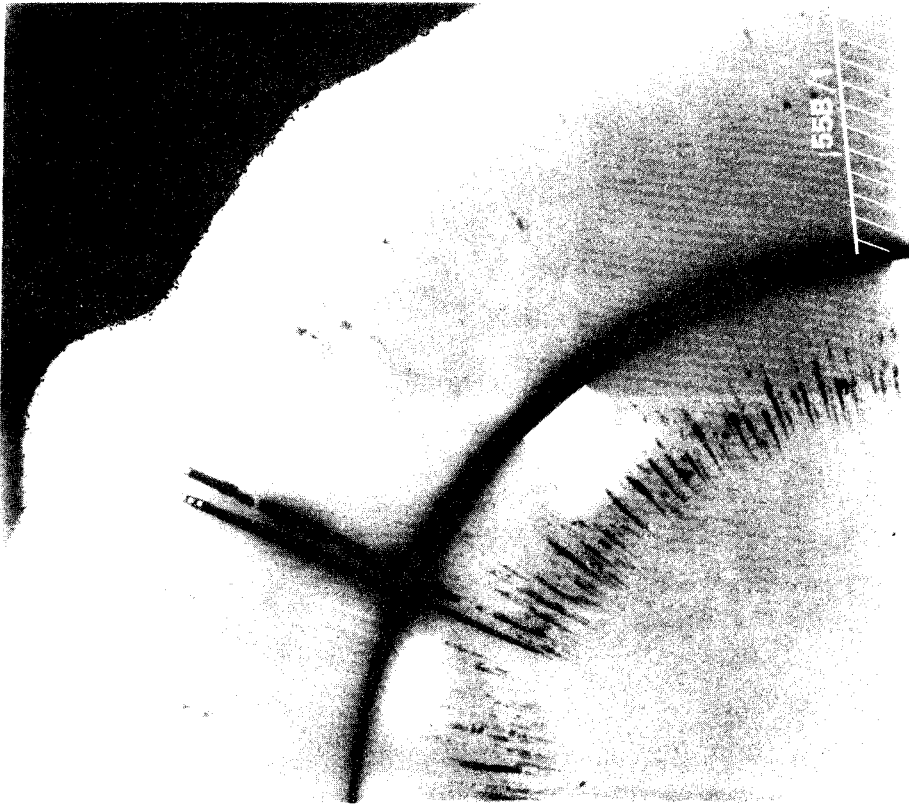
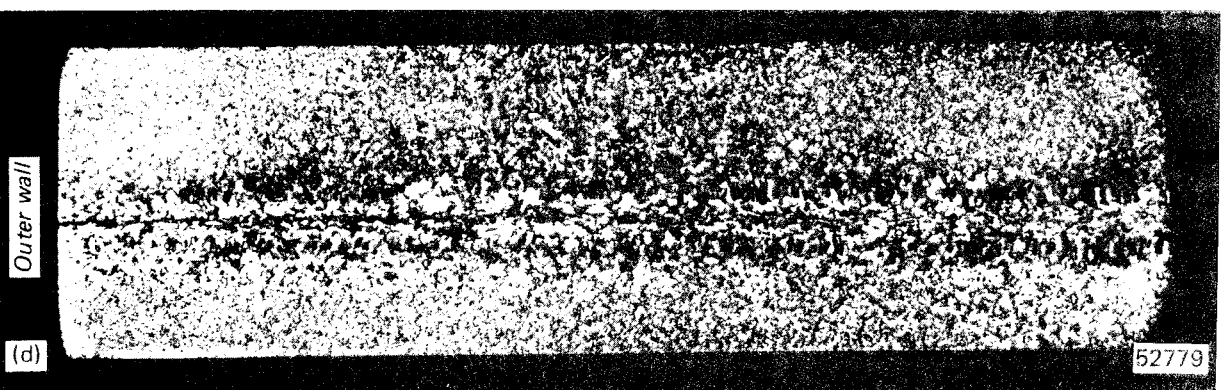
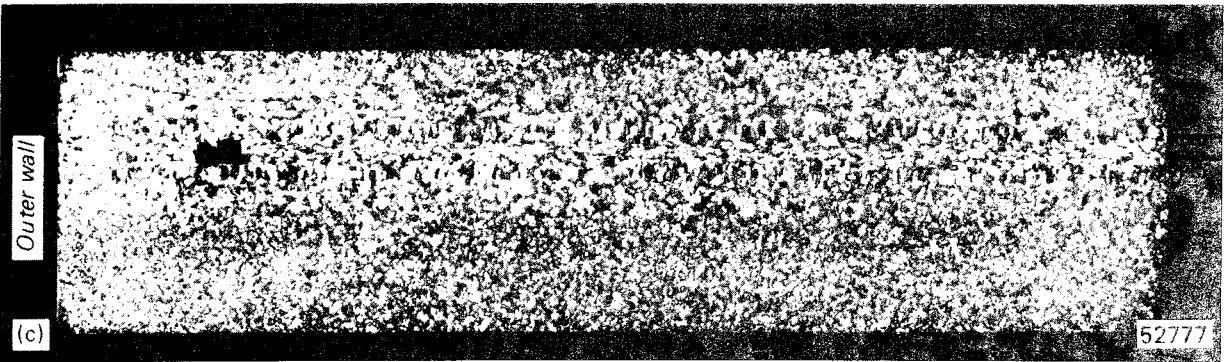
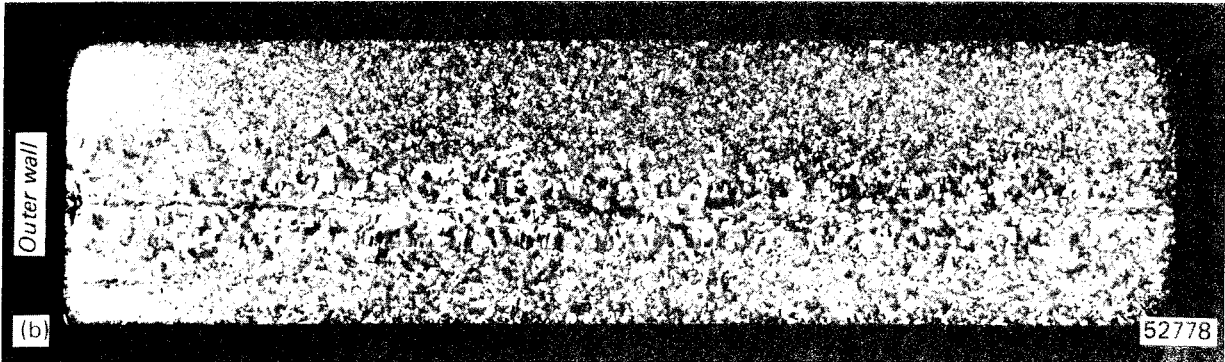
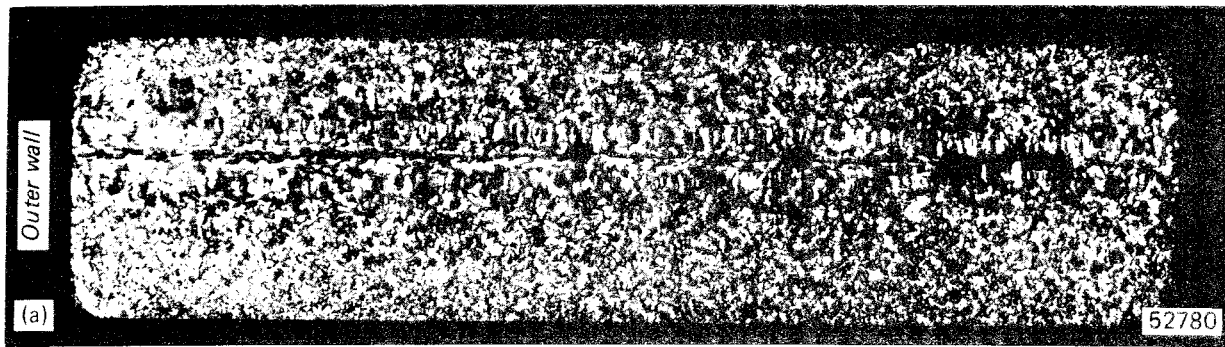


Fig.25. Radiographs of simulated lid weld:  
a) quadrant DOC showing 'shut-down' and root defects b) quadrant AOB showing 'fade-out' defects.



*Fig.26. Transverse macrosections taken from simulated lid weld:*

- a) specimen 55A/1 – showing large pores at start of beam fade-out region*
- b) specimen 55A/2 – showing small central defects and pores in upper region*
- c) specimen 55A/3 – showing pore in upper region*
- d) specimen 55B/1 – showing no defects; see Fig.23 to 25. All macros, x1.6.*

## RESIDUAL STRESS MEASUREMENTS IN AN EB WELDED COPPER DISC

By: R. H. Leggatt

INTRODUCTION

The Welding Institute have carried out a trial electron beam weld on a solid copper disc of diameter 600mm and total thickness 200mm. The sponsors, SKBF, wished to have some information on the residual stresses likely to be present in such a weld. A literature search on the "Weldasearch" system revealed no relevant data. It was therefore decided to make some surface stress measurements on the welded copper discs using the centre hole technique.

SPECIMEN

The specimen design and welding procedures are described in a separate report (Ref. LD 22965). The trial weld was intended to model the closing joint between the lid and body of a heavy section cylindrical canister. The lid was represented by two discs of diameters 600mm and 400mm and thickness 100mm each. The smaller disc fitted into a 20mm deep recess in one face of the larger disc. The body of the canister was represented by an annulus of inner diameter 400mm, outer diameter 600mm, and thickness (in the axial direction) of 100mm. The annulus fitted over the smaller disc and was welded to the larger disc by means of a circumferential EB weld. A cross-section of the joint (after the specimen had been reduced in diameter and sawn into quadrants) is shown in Fig. 1d.

EXPERIMENTAL PROCEDURE

Residual stresses were measured using centre hole rosette gauges. The hole was formed using a rotating air abrasive jet. The hole diameter and depth were approximately 2.0mm. Full details of the equipment, procedures and calibration factors are given by Beaney [1], who quotes an accuracy of  $\pm 8\%$  for stresses below 65% of yield.

The gauge locations are shown on Fig. 1. Gauges 1 to 5 were attached to the outer surface of the specimen as-received after welding. The specimen was then reduced to a diameter of 588mm on a lathe. Gauges 6 to 9 were applied on the machined surface, and gauge 10 on the side face. Finally, the specimen was cut into four quadrants. The sawn surface of one quadrant was prepared for gauging by removing material to a depth of 0.25mm with a hand held rotary polisher using a fine grit wheel. This preparation procedure was intended to remove any surface effects induced by sawing. Gauges 11 to 14 were applied to the EB weld metal on the exposed cross section.

## RESULTS

The results were calculated using a Young's modulus value of  $118,000 \text{ N/mm}^2$  [2] and  $\nu_{K_2/K_1} = 0.3$  ( $\nu_{K_2/K_1}$  is a centre hole constant closely related to Poisson's ratio).

The results are listed in Table 1 and are plotted on Fig. 2. All the measured stresses were small, in the range  $-32$  to  $+36 \text{ N/mm}^2$ . The stresses on the disc as-welded were compressive, except at the measurement point 10mm from the weld where a hoop tensile stress of  $11 \text{ N/mm}^2$  was found.

The stresses measured after machining the outside diameter were in all cases more tensile than those in the as-welded condition. In the case of the stresses on the side face of the disc, which was not machined, the stress changes were negligible. However, there were significant stress changes on the outside diameter, averaging  $+22 \text{ N/mm}^2$  in the hoop direction and  $+10 \text{ N/mm}^2$  in the direction transverse to the weld. The peak tensile stresses were on the weld itself:  $32 \text{ N/mm}^2$  in the hoop direction and  $19 \text{ N/mm}^2$  in the transverse direction.

The stresses on the weld cross section after cutting the disc assembly into quadrants were even smaller than those on the external face, and lay in the range  $-16 \text{ N/mm}^2$  to  $3 \text{ N/mm}^2$ .

## DISCUSSION

The possible causes of residual stresses in the welded copper disc specimens are weld shrinkage, non-uniform cooling and machining stresses. In steel weldments, weld shrinkage usually causes yield magnitude tensile residual stresses in the weld and adjacent parent material. In the present specimen, the peak tensile stresses were found in weld metal, and these stresses may be assumed to have been caused by weld shrinkage. The maximum measured stress was  $36 \text{ N/mm}^2$ , which may be compared with published values of 0.1% proof stress for oxygen free coppers, which lie in the range  $45 \text{ N/mm}^2$  to  $320 \text{ N/mm}^2$  [2], depending on condition, product and the degree of hot and cold working. As the fused metal is effectively hot worked as it tries to contract, it seems likely that its proof stress would be similar to that of hot worked products, i.e.  $90 \text{ N/mm}^2$ . The maximum measured residual stress was significantly lower than this, presumably due to the fact that the disc specimen reached a mean temperature of about  $400^\circ\text{C}$  soon after welding was completed. At this temperature the yield stress is very low, and large weld shrinkage stresses cannot be sustained. Once a uniform temperature is achieved there is no further differential weld shrinkage, and no additional weld shrinkage stress can be generated.

However, additional residual stresses can arise if the disc is allowed to cool in a non-uniform manner. In the present instance, air was allowed into the vacuum chamber whilst the disc was still at a temperature of about  $400^\circ\text{C}$ . Rapid surface cooling can cause the outer

surface of a massive body to yield in tension. On final cooling of the core the surface layer goes into compression. Fig. 2a shows that there were surface compressive stresses in the range  $-13$  to  $-29$  N/mm<sup>2</sup> on the side face of the discs. Fig. 2b shows that the stresses on the outer surface before machining were more compressive than those measured after the surface had been removed. The stress differences at particular locations were in the range  $-5$  to  $-33$  N/mm<sup>2</sup>. Both results suggest that air cooling did cause compressive surface stresses in the disc. These stresses were superimposed on the weld induced stresses on the outer diameter. Compressive surface stresses are beneficial in inhibiting any tendency for stress corrosion cracking.

Other possible sources of residual stresses are the machining and preparation processes applied to the surface prior to application of the gauges. Such stresses would mask the effects of weld shrinkage and cooling stresses. In view of the consistency of the surface compression effects described above, it appears that the reduction of the diameter on the lathe did not cause any significant machining stresses.

It is not possible to state whether the sawing and polishing applied to the weld cross-section specimen had any effect on the measured stresses shown on Fig. 2c. Having found a tensile axial stress on the outer surface before sawing ( $19$  N/mm<sup>2</sup>) it was expected that similar or higher stresses might have been found inside the weld. However, any such stresses would have been affected both by the sectioning of the specimen, which relieved the normal and shear stresses on the cut faces, and by the machining process itself. In spite of these unknown stress changes during cutting it would be expected that any large internal axial or radial stresses in the weld would produce significant remnant stresses on the cut face. The measured stresses were in fact very low (maximum  $3$  N/mm<sup>2</sup>), which suggests that no large internal stresses were present before cutting.

## CONCLUSIONS

The measured residual stresses on the EB welded copper disc lay in the range  $-32$  N/mm<sup>2</sup> to  $+36$  N/mm<sup>2</sup>. The peak tensile stresses were found on the weld itself after removal of the outer layer of material, and were caused by weld shrinkage. The peak stress was less than half the assumed value of the proof stress of the fused metal. The surface of the specimen contained compressive stresses of up to  $-29$  N/mm<sup>2</sup> which were probably caused by rapid air cooling after welding.

## ACKNOWLEDGEMENTS

The experimental work was carried out by Mr. B. A. Martin of the Design Advisory Section. The author is grateful for the co-operation of Dr. A. Sanderson of the EB welding section.

*R. H. Leggatt*

#### REFERENCES

1. BEANEY, E.M. "Accurate measurement of residual stresses on any steel using the centre-hole method", Strain, July 1976, p. 99.
2. STAMFORD, M.S. "Copper data", The Copper Development Association, Technical Note TN20, 1975.

TABLE 1 Residual stress measurements

Gauge No.	Hole dia. mm	Stresses in N/mm <sup>2</sup>					$\theta$
		$\sigma_{\min}$	$\sigma_{\max}$	axial	hoop	radial	
1	1.98	-3	15	1	11		119
2	1.98	-28	-5	-11	-22		30
3	2.02	-12	1	-1	-11		21
4	1.99	-30	-10		-14	-26	117
5	1.98	-32	-11		-15	-29	114
6	2.05	15	36	19	32		64
7	2.03	6	24	9	21		66
8	2.09	2	16	6	11		55
9	2.09	4	11	4	11		78
10	2.08	-25	-10		-13	-22	116
11	1.98	-16	-3	-5		-14	68
12	1.95	-6	2	1		-5	103
13	1.96	-10	-2	-7		-6	43
14	1.96	-10	3	3		-10	91

$\theta$  is the angle in degrees of maximum principal stress measured clockwise from gauge element 1. The gauge element orientation is shown on Fig. 1.

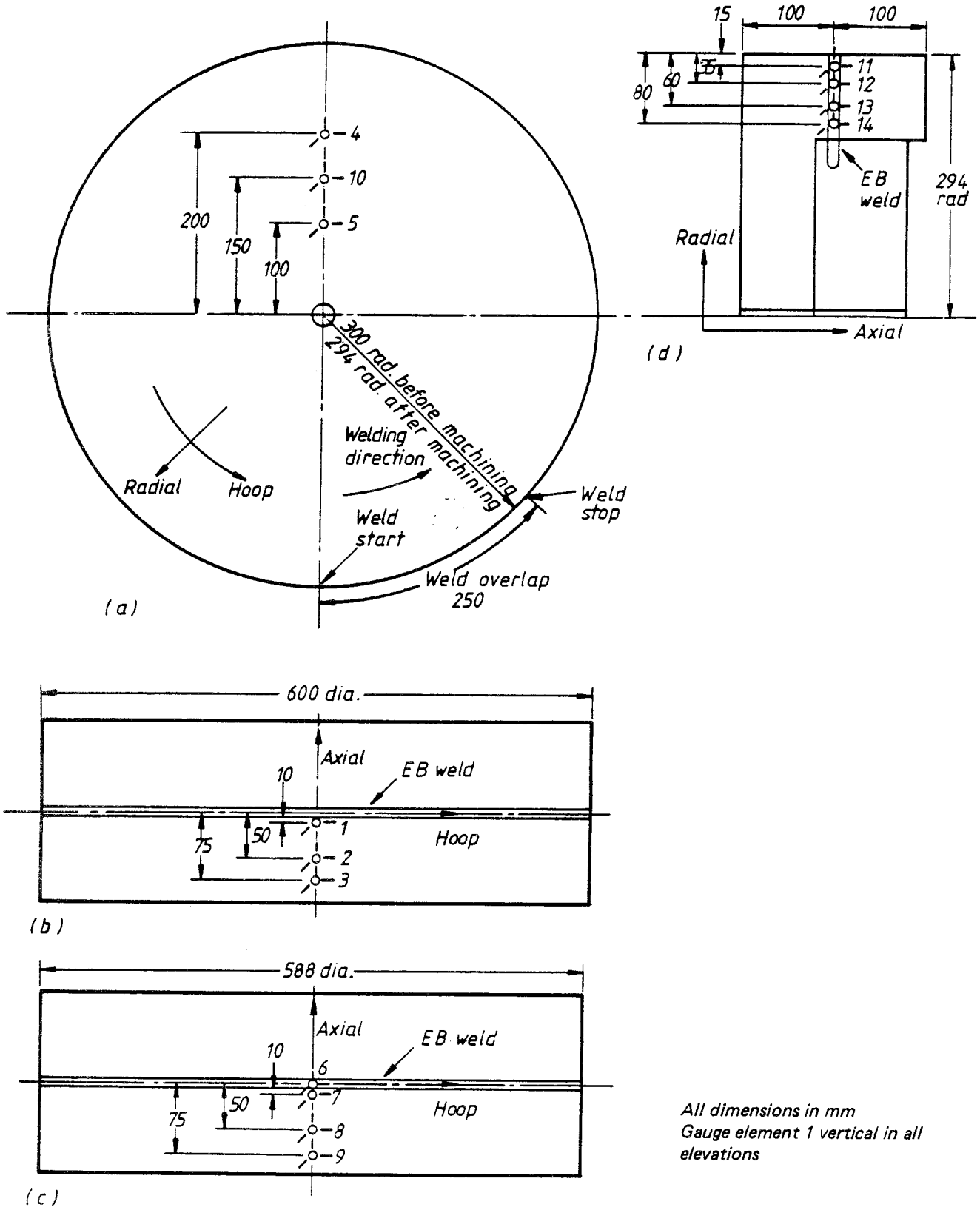


Fig.1. Centre hole gauge locations:

a) on flat side face    b) on outside diameter before machining    c) on outside diameter after machining  
d) on weld cross-section after sawing into quadrants

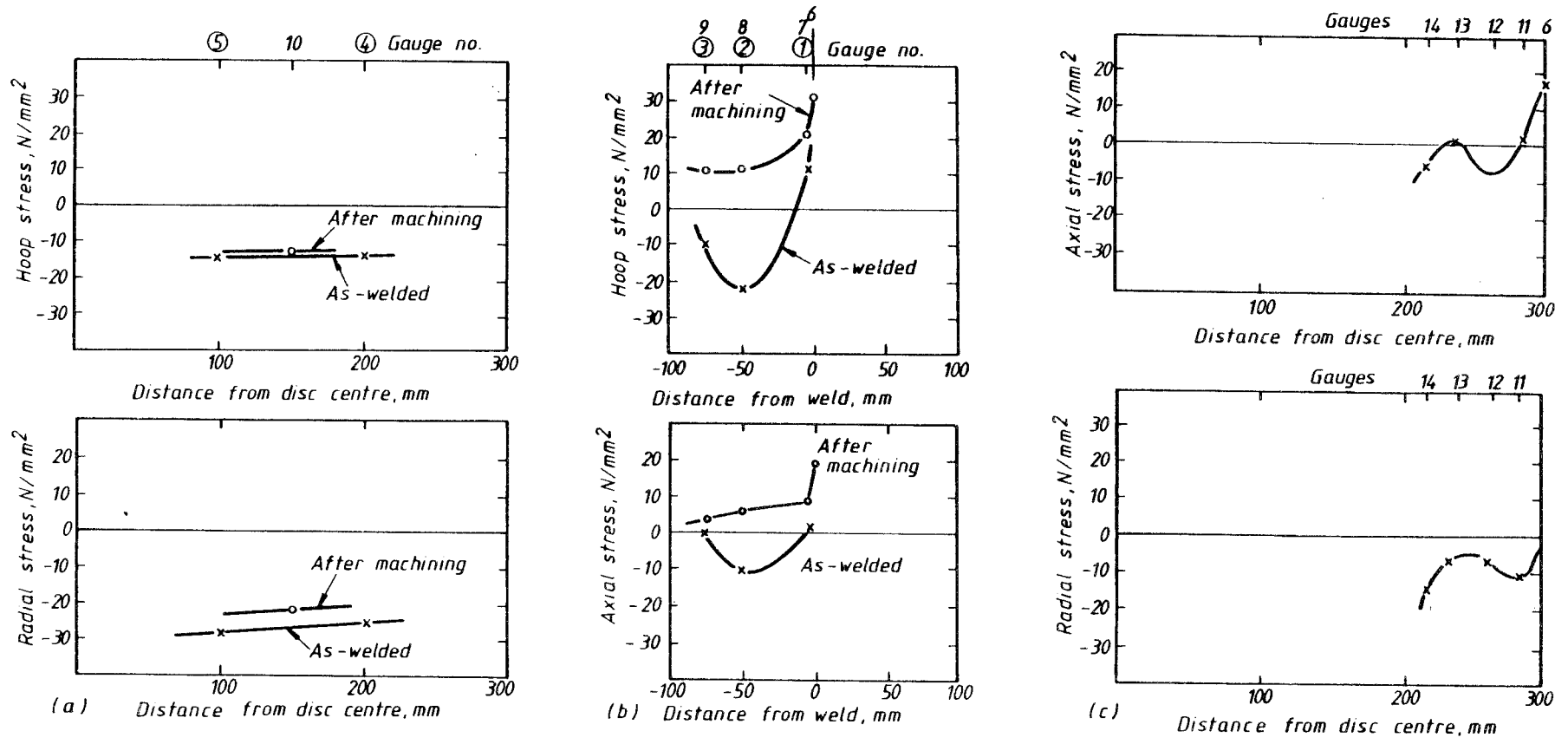


Fig.2. Residual stresses before and after machining:  
 a) on side face    b) on outside diameter    c) on weld cross-section

LIST OF KBS's TECHNICAL REPORTS

1977-78

TR 121 KBS Technical Reports 1 - 120.  
Summaries. Stockholm, May 1979.

1979

TR 79-28 The KBS Annual Report 1979.  
KBS Technical Reports 79-01--79-27.  
Summaries. Stockholm, March 1980.

1980

TR 80-26 The KBS Annual Report 1980.  
KBS Technical Reports 80-01--80-25.  
Summaries. Stockholm, March 1981.

1981

TR 81-17 The KBS Annual Report 1981.  
KBS Technical Reports 81-01--81-16  
Summaries. Stockholm, April 1982.

1983

TR 83-01 Radionuclide transport in a single fissure  
A laboratory study  
Trygve E Eriksen  
Department of Nuclear Chemistry  
The Royal Institute of Technology  
Stockholm, Sweden 1983-01-19

TR 83-02 The possible effects of alfa and beta radiolysis  
on the matrix dissolution of spent nuclear fuel  
I Grenthe  
I Puigdomènech  
J Bruno  
Department of Inorganic Chemistry  
Royal Institute of Technology  
Stockholm, Sweden January 1983

- TR 83-03 Smectite alteration  
Proceedings of a colloquium at State University of  
New York at Buffalo, May 26-27, 1982  
Compiled by Duwayne M Anderson  
State University of New York at Buffalo  
February 15, 1983
- TR 83-04 Stability of bentonite gels in crystalline rock -  
Physical aspects  
Roland Pusch  
Division Soil Mechanics, University of Luleå  
Luleå, Sweden, 1983-02-20
- TR 83-05 Studies in pitting corrosion on archeological  
bronzes - Copper  
Åke Bresle  
Jozef Saers  
Birgit Arrhenius  
Archaeological Research Laboratory  
University of Stockholm  
Stockholm, Sweden 1983-01-02
- TR 83-06 Investigation of the stress corrosion cracking of  
pure copper  
L A Benjamin  
D Hardie  
R N Parkins  
University of Newcastle upon Tyne  
Department of Metallurgy and Engineering Materials  
Newcastle upon Tyne, Great Britain, April 1983
- TR 83-07 Sorption of radionuclides on geologic media -  
A literature survey. I: Fission Products  
K Andersson  
B Allard  
Department of Nuclear Chemistry  
Chalmers University of Technology  
Göteborg, Sweden 1983-01-31
- TR 83-08 Formation and properties of actinide colloids  
U Olofsson  
B Allard  
M Bengtsson  
B Torstenfelt  
K Andersson  
Department of Nuclear Chemistry  
Chalmers University of Technology  
Göteborg, Sweden 1983-01-30
- TR 83-09 Complexes of actinides with naturally occurring  
organic substances - Literature survey  
U Olofsson  
B Allard  
Department of Nuclear Chemistry  
Chalmers University of Technology  
Göteborg, Sweden 1983-02-15
- TR 83-10 Radiolysis in nature:  
Evidence from the Oklo natural reactors  
David B Curtis  
Alexander J Gancarz  
New Mexico, USA February 1983

- TR 83-11 Description of recipient areas related to final storage of unprocessed spent nuclear fuel  
Björn Sundblad  
Ulla Bergström  
Studsvik Energiteknik AB  
Nyköping, Sweden 1983-02-07
- TR 83-12 Calculation of activity content and related properties in PWR and BWR fuel using ORIGEN 2  
Ove Edlund  
Studsvik Energiteknik AB  
Nyköping, Sweden 1983-03-07
- TR 83-13 Sorption and diffusion studies of Cs and I in concrete  
K Andersson  
B Torstenfelt  
B Allard  
Department of Nuclear Chemistry  
Chalmers University of Technology  
Göteborg, Sweden 1983-01-15
- TR 83-14 The complexation of Eu(III) by fulvic acid  
J A Marinsky  
State University of New York at Buffalo, Buffalo, NY  
1983-03-31
- TR 83-15 Diffusion measurements in crystalline rocks  
Kristina Skagius  
Ivars Neretnieks  
Royal Institute of Technology  
Stockholm, Sweden 1983-03-11
- TR 83-16 Stability of deep-sited smectite minerals in crystalline rock - chemical aspects  
Roland Pusch  
Division of Soil Mechanics, University of Luleå  
1983-03-30
- TR 83-17 Analysis of groundwater from deep boreholes in Gideå Sif Laurent  
Swedish Environmental Research Institute  
Stockholm, Sweden 1983-03-09
- TR 83-18 Migration experiments in Studsvik  
O Landström  
Studsvik Energiteknik AB  
C-E Klockars  
O Persson  
E-L Tullborg  
S Å Larson  
Swedish Geological  
K Andersson  
B Allard  
B Torstenfelt  
Chalmers University of Technology  
1983-01-31

- TR 83-19 Analysis of groundwater from deep boreholes in Fjällveden  
Sif Laurent  
Swedish Environmental Research Institute  
Stockholm, Sweden 1983-03-29
- TR 83-20 Encapsulation and handling of spent nuclear fuel for final disposal  
1 Welded copper canisters  
2 Pressed copper canisters (HIPOW)  
3 BWR Channels in Concrete  
B Lönnerberg, ASEA-ATOM  
H Larker, ASEA  
L Ageskog, VBB  
May 1983
- TR 83-21 An analysis of the conditions of gas migration from a low-level radioactive waste repository  
C Braester  
Israel Institute of Technology, Haifa, Israel  
R Thunvik  
Royal Institute of Technology, Stockholm, Sweden  
November 1982
- TR 83-22 Calculated temperature field in and around a repository for spent nuclear fuel  
Taivo Tarandi, VBB  
Stockholm, Sweden April 1983
- TR 83-23 Preparation of titanates and zeolites and their uses in radioactive waste management, particularly in the treatment of spent resins  
Å Hultgren, editor  
C Airola  
Studsvik Energiteknik AB  
S Forberg, Royal Institute of Technology  
L Fälth, University of Lund  
May 1983
- TR 83-24 Corrosion resistance of a copper canister for spent nuclear fuel  
The Swedish Corrosion Research Institute and its reference group  
Stockholm, Sweden April 1983
- TR 83-25 Feasibility study of electron beam welding of spent nuclear fuel canisters  
A Sanderson, T F Szluha, J L Turner, R H Leggatt  
The Welding Institute  
Cambridge, The United Kingdom April 1983
- TR 83-26 The KBS UO<sub>2</sub> leaching program  
Summary Report 1983-02-01  
Ronald Forsyth, Studsvik Energiteknik AB  
Nyköping, Sweden February 1983
- TR 83-27 Radiation effects on the chemical environment in a radioactive waste repository  
Trygve Eriksen  
Royal Institute of Technology, Stockholm  
Arvid Jacobsson  
University of Luleå, Luleå  
Sweden 1983-07-01

- TR 83-28 An analysis of selected parameters for the  
BIOPATH-program  
U Bergström  
A-B Wilkens  
Studsvik Energiteknik AB  
Nyköping, Sweden 1983-06-08
- TR 83-29 On the environmental impact of a repository for  
spent nuclear fuel  
Otto Brotzen  
Stockholm, Sweden April 1983
- TR 83-30 Encapsulation of spent nuclear fuel -  
Safety Analysis  
ES-konsult AB  
Stockholm, Sweden April 1983
- TR 83-31 Final disposal of spent nuclear fuel -  
Standard programme for site investigations  
Compiled by  
Ulf Thoregren  
Swedish Geological  
April 1983
- TR 83-32 Feasibility study of detection of defects in thick  
welded copper  
Tekniska Röntgencentralen AB  
Stockholm, Sweden April 1983
- TR 83-33 The interaction of bentonite and glass with  
aqueous media  
M Mosslehi  
A Lambrosa  
J A Marinsky  
State University of New York  
Buffalo, NY, USA April 1983
- TR 83-34 Radionuclide diffusion and mobilities in compacted  
bentonite  
B Torstenfelt  
B Allard  
K Andersson  
H Kipatsi  
L Eliasson  
U Olofsson  
H Persson  
Chalmers University of Technology  
Göteborg, Sweden April 1983
- TR 83-35 Actinide solution equilibria and solubilities in  
geologic systems  
B Allard  
Chalmers University of Technology  
Göteborg, Sweden 1983-04-10
- TR 83-36 Iron content and reducing capacity of granites and  
bentonite  
B Torstenfelt  
B Allard  
W Johansson  
T Ittner  
Chalmers University of Technology  
Göteborg, Sweden April 1983

- TR 83-37 Surface migration in sorption processes  
A Rasmuson  
I Neretnieks  
Royal Institute of Technology  
Stockholm, Sweden March 1983
- TR 83-38 Evaluation of some tracer tests in the granitic  
rock at Finnsjön  
L Moreno  
I Neretnieks  
Royal Institute of Technology, Stockholm  
C-E Klockars  
Swedish Geological, Uppsala  
April 1983
- TR 83-39 Diffusion in the matrix of granitic rock  
Field test in the Stripa mine. Part 2  
L Birgersson  
I Neretnieks  
Royal Institute of Technology  
Stockholm, Sweden March 1983
- TR 83-40 Redox conditions in groundwaters from  
Svartboberget, Gideå, Fjällveden and Kamlunge  
P Wikberg  
I Grenthe  
K Axelsen  
Royal Institute of Technology  
Stockholm, Sweden 1983-05-10
- TR 83-41 Analysis of groundwater from deep boreholes in  
Svartboberget  
Sif Laurent  
Swedish Environmental Research Institute  
Stockholm, Sweden 1983-06-10
- TR 83-42 Final disposal of high-level waste and spent  
nuclear fuel - foreign activities  
R Gelin  
Studsvik Energiteknik AB  
Nyköping, Sweden May 1983
- TR 83-43 Final disposal of spent nuclear fuel - geological,  
hydrological and geophysical methods for site  
characterization  
K Ahlbom  
L Carlsson  
O Olsson  
Swedish Geological  
Sweden May 1983
- TR 83-44 Final disposal of spent nuclear fuel - equipment  
for site characterization  
K Almén, K Hansson, B-E Johansson, G Nilsson  
Swedish Geological  
O Andersson, IPA-Konsult  
P Wikberg, Royal Institute of Technology  
H Åhagen, SKBF/KBS  
May 1983

- TR 83-45 Model calculations of the groundwater flow at Finnsjön, Fjällveden, Gideå and Kamlunga  
L Carlsson  
A Winberg  
Swedish Geological, Göteborg  
B Grundfelt  
Kemakta Consultant Company, Stockholm  
May 1983
- TR 83-46 Use of clays as buffers in radioactive repositories  
Roland Pusch  
University of Luleå  
Luleå May 25 1983
- TR 83-47 Stress/strain/time properties of highly compacted bentonite  
Roland Pusch  
University of Luleå  
Luleå May 1983
- TR 83-48 Model calculations of the migration of radionuclides from a repository for spent nuclear fuel  
A Bengtsson  
Kemakta Consultant Company, Stockholm  
M Magnusson  
I Neretnieks  
A Rasmuson  
Royal Institute of Technology, Stockholm  
May 1983
- TR 83-49 Dose and dose commitment calculations from groundwaterborne radioactive elements released from a repository for spent nuclear fuel  
U Bergström  
Studsvik Energiteknik AB  
Nyköping, Sweden May 1983
- TR 83-50 Calculation of fluxes through a repository caused by a local well  
R Thunvik  
Royal Institute of Technology  
Stockholm, Sweden May 1983
- TR 83-51 GWHRT - A finite element solution to the coupled ground water flow and heat transport problem in three dimensions  
B Grundfelt  
Kemakta Consultant Company  
Stockholm, Sweden May 1983
- TR 83-52 Evaluation of the geological, geophysical and hydrogeological conditions at Fjällveden  
K Ahlbom  
L Carlsson  
L-E Carlsten  
O Duran  
N-Å Larsson  
O Olsson  
Swedish Geological  
May 1983

- TR 83-53 Evaluation of the geological, geophysical and hydrogeological conditions at Gideå  
K Ahlbom  
B Albino  
L Carlsson  
G Nilsson  
O Olsson  
L Stenberg  
H Timje  
Swedish Geological  
May 1983
- TR 83-54 Evaluation of the geological, geophysical and hydrogeological conditions at Kamlunge  
K Ahlbom  
B Albino  
L Carlsson  
J Danielsson  
G Nilsson  
O Olsson  
S Sehlstedt  
V Stejskal  
L Stenberg  
Swedish Geological  
May 1983
- TR 83-55 Evaluation of the geological, geophysical and hydrogeological conditions at Svartboberget  
K Ahlbom  
L Carlsson  
B Gentzschein  
A Jämtlid  
O Olsson  
S Tirén  
Swedish Geological  
May 1983
- TR 83-56 I: Evaluation of the hydrogeological conditions at Finnsjön  
II: Supplementary geophysical investigations of the Sternö peninsula  
B Hesselström  
L Carlsson  
G Gidlund  
Swedish Geological  
May 1983
- TR 83-57 Neotectonics in northern Sweden - geophysical investigations  
H Henkel  
K Hult  
L Eriksson  
Geological Survey of Sweden  
L Johansson  
Swedish Geological  
May 1983

- TR 83-58 Neotectonics in northern Sweden - geological investigations  
R Lagerbäck  
F Witschard  
Geological Survey of Sweden  
May 1983
- TR 83-59 Chemistry of deep groundwaters from granitic bedrock  
B Allard  
Chalmers University of Technology  
S Å Larson  
E-L Tullborg  
Swedish Geological  
P Wikberg  
Royal Institute of Technology  
May 1983
- TR 83-60 On the solubility of technetium in geochemical systems  
B Allard  
B Torstenfelt  
Chalmers University of Technology  
Göteborg, Sweden 1983-05-05
- TR 83-61 Sorption behaviour of well-defined oxidation states  
B Allard  
U Olofsson  
B Torstenfelt  
H Kipatsi  
Chalmers University of Technology  
Göteborg, Sweden 1983-05-15
- TR 83-62 The distribution coefficient concept and aspects on experimental distribution studies  
B Allard  
K Andersson  
B Torstenfelt  
Chalmers University of Technology  
Göteborg, Sweden May 1983
- TR 83-63 Sorption of radionuclides in geologic systems  
K Andersson  
B Torstenfelt  
B Allard  
Chalmers University of Technology  
Göteborg, Sweden 1983-06-15
- TR 83-64 Ion exchange capacities and surface areas of some major components and common fracture filling materials of igneous rocks  
B Allard  
M Karlsson  
Chalmers University of Technology  
E-L Tullborg  
S Å Larson  
Swedish Geological  
Göteborg, Sweden May 1983

- TR 83-65 Sorption of actinides on uranium dioxide and zirconium dioxide in connection with leaching of uranium dioxide fuel  
B Allard  
N Berner  
K Andersson  
U Olofsson  
B Torstenfelt  
Chalmers University of Technology  
R Forsyth  
Studsvik Energiteknik AB  
May 1983
- TR 83-66 The movement of radionuclides past a redox front  
I Neretnieks  
B Åslund  
Royal Institute of Technology  
Stockholm, Sweden 1983-04-22
- TR 83-67 Some notes in connection with the studies of final disposal of spent fuel. Part 2  
I Neretnieks  
Royal Institute of Technology  
Stockholm, Sweden May 1983
- TR 83-68 Two dimensional movements of a redox front downstream from a repository for nuclear waste  
I Neretnieks  
B Åslund  
Royal Institute of Technology  
Stockholm, Sweden 1983-06-03
- TR 83-69 An approach to modelling radionuclide migration in a medium with strongly varying velocity and block sizes along the flow path  
I Neretnieks  
A Rasmuson  
Royal Institute of Technology  
Stockholm, Sweden May 1983
- TR 83-70 Analysis of groundwater from deep boreholes in Kamlunge  
S Laurent  
Swedish Environmental Research Institute  
Stockholm, Sweden May 1983
- TR 83-71 Gas migration through bentonite clay  
Roland Fusch  
Thomas Forsberg  
University of Luleå  
Luleå, Sweden May 31, 1983